Forschungszentrum Karlsruhe
Technik und Umwelt

Wissenschaftliche Berichte
FZKA 6675

Development, Implementation and Verification of a Reduced Hydrogen-Air Chemistry Model for the COM3D Computer Code

Z. Xu, A. Kotchourko

Institut für Kern- und Energietechnik
Programm Nukleare Sicherheitsforschung

November 2001

Forschungszentrum Karlsruhe

Technik und Umwelt

Wissenschaftliche Berichte

FZKA 6675

Development, Implementation and Verification of a Reduced Hydrogen-Air Chemistry Model for the COM3D Computer Code

Zhanjie Xu, Alexei Kotchourko

Institut für Kern- und Energietechnik

Programm Nukleare Sicherheitsforschung

Forschungszentrum Karlsruhe GmbH, Karlsruhe
2001

Forschungszentrum Karlsruhe GmbH
Postfach 3640, 76021 Karlsruhe

Mitglied der Hermann von Helmholtz-Gemeinschaft
Deutscher Forschungszentren (HGF)

ISSN 0947-8620

Abstract

Development, Implementation and Verification of a Reduced Hydrogen-Air Chemistry Model for the COM3D Computer Code

The primary objective of this work was to develop a fast-running but still sufficiently precise chemistry model for use in three-dimensional CFD programs.

For this aim a new approach to simplify detailed schemes was proposed. The main assumption of this approach is that the species concentrations, the species consumption and production rates during chemical reactions with the reduced scheme share the same values with the detailed scheme under the same initial condition and at the identical time moment for an adiabatic homogeneous closed system. Then the reaction rate constants of the reduced scheme can be fitted using polynomials. As an example, a seven-step detailed scheme is reduced to a two-step scheme, which is chosen because it represents the mechanism of chain-branching and radical-terminating in the simplest way. The reaction rate constants of the two reactions are derived from the seven-step scheme and fitted in the form of fast evaluating polynomials. The derived reduced scheme has quite wide range of applicability and good agreement with the detailed scheme in views of the induction time and the reaction time.

The new reduced scheme was implemented into the COM3D code and experiments were performed to validate the computer code. The comparison between the experiments and the corresponding calculations demonstrated that the code with the new reduced chemistry can reproduce all essential behaviors of the lean or stoichiometric hydrogen-air mixture in a very satisfactory way. Many test calculations demonstrated the numerical stability, convergence and fast-running performance of the code updated with the new reduced chemistry. It may be concluded that the new COM3D version can correctly predict the dynamics of a large range of hydrogen-oxygen combustion regimes, from slow deflagration to detonation.

Zusammenfassung

Entwicklung, Implementierung und Verifikation eines reduzierten H_2-Luft-Chemiemodells für das COM3D-Rechenprogramm

Das grundlegende Ziel dieser Arbeit war die Entwicklung eines schnellen und dabei hinreichend genauen chemischen Modells für die Nutzung in dreidimensionalen CFD-Programmen.

Zu diesem Zweck wurde eine neue Herangehensweise zur Vereinfachung detaillierter Schemata vorgeschlagen. Die wesentliche Annahme dieser Methode sind gleiche Konzentrationen, Verbrauchs- und Produktionsraten der Spezies während der chemischen Reaktionen im detaillierten wie im reduzierten Schema bei gleichen Anfangsbedingungen und Zeitpunkten in einem adiabatischen homogenen geschlossenen System. Die Konstanten für die Reaktionsraten des reduzierten Schemas können dann durch Polynome angenähert werden. Als Beispiel wurde ein detailliertes Schema mit sieben Schritten auf ein Schema mit zwei Schritten reduziert. Das Schema wurde gewählt, weil es die Mechanismen von Ketten-Verzweigung und Kettenabbruch für den einfachsten Fall darstellt. Die Konstanten der Reaktionsraten für beide Reaktionen sind vom Sieben-Schritt-Schema abgeleitet und in Form von schnell auswertbaren Polynomen angepasst worden. Das abgeleitete reduzierte Schema hat einen recht großen Anwendungsbereich und ist in guter Übereinstimmung mit dem detaillierten Schema in Hinsicht auf die Induktions- und Reaktionszeit.

Das neue reduzierte Schema wurde in das COM3D-Programm implementiert und es wurden Experimente durchgeführt, um das Programm zu validieren. Der Vergleich zwischen den Experimenten und den zugehörigen Berechnungen zeigt, dass das Programm mit der neuen reduzierten Chemie das gesamte wesentliche Verhalten des mageren und des stöchiometrischen H_2-Luft-Gemisches auf recht zufriedenstellende Weise reproduzieren kann. Viele Testrechnungen demonstrieren numerische Stabilität, Konvergenz und schnelle Ausführung des mit der neuen reduzierten Chemie aktualisierten Programms. Es kann geschlussfolgert werden, dass die neue COM3D-Version die Dynamik in einem großen Bereich des H_2-O_2-Verbrennungsregimes voraussagen kann, von langsamer Deflagration bis hin zur Detonation.

CONTENTS

1. Introduction

There is a general conclusion that in the coming few decades, computer techniques would be still inadequate to solve the problem of reactive flow with detailed chemistry when geometric complexity and turbulence are considered [1]. So it is necessary to develop methods to simplify the detailed kinetics scheme mathematically or numerically without significant loss of accuracy [2]. Partial equilibrium and steady state assumption methods are used to realize this aim traditionally [3~12]. However, the quasi-equilibriums or steady-state assumptions might vary with different initial conditions of the reactive flow system, such as composition, temperature, pressure and even the specific way of mixing between fuel and oxygen. Therefore, in most cases the reduced schemes obtained by such methods have relatively narrow application ranges. They are applicable only in some restricted range of initial conditions.

In recent years an intrinsic low-dimensional manifold (ILDM) method [13] was proposed to simplify detailed chemistry. By means of eigen value analysis, which is a completely mathematical method, those elementary reactions with fast time scale can be eliminated, and a lower dimensional reaction sub-space can be obtained. According to the literature [13], a mathematical table about species reaction rates under given initial parameters of the mixture can be obtained by the ILDM method. In applications, the table can be embedded into a computer code and the concerned reaction rates can be obtained by table-lookup and/or interpolation. The advantage of ILDM is that it can be used to simplify the detailed chemistry scheme effectively and most reasonably, without any assumptions or expert opinions on chemistry because it is of totally mathematical nature.

In this paper, a new numerical method is proposed to reduce the detailed chemistry. The formulas of reaction rate constants of the controlling reactions after simplification, instead of multi-dimensional tables, are gained from analytical formulas. The hydrogen-air system is taken as an example and polynomials with no more than 17 terms are obtained to fit the reaction rate constants in wide ranges of pressure, temperature and mixture composition. The following section formulates the method in detail. Then the hydrogen-air system is taken as an example to show the process of numerical fitting. Next the reduced scheme is implemented into the COM3D computer code, and finally the calculation results are compared with the real data from experiments. The conclusions are presented in the last chapter.

2. Reduction method

First, a detailed scheme is applied to an adiabatic homogeneous closed system to calculate the species concentrations, production rates and consumption rates during chemical reaction under different initial conditions. It is obvious that, the more accurate the detailed scheme is, and the wider its application range is, the better the model is. That is, the accuracy and the application range of the reduced scheme, which is developed based on the detailed scheme, depend on the quality of the detailed scheme.

Second, steady-state approximations for the species being not concerned are introduced into the detailed chemical equations. A reduced scheme with much fewer

reaction steps can be produced. It should be explained that the method of steady-state approximations is adopted here only to simplify the chemical equations. Normally it is quite easy to eliminate those chemical species being not considered from the original detailed chemical equations. The reaction rates of the reduced scheme are obtained not by the steady-state method but by a numerical approach. The reduced scheme should be so simple that the number of reaction steps is not greater than the number of species involved in the chemical equations. Here a reaction with forward and backward directions is counted as one step. Normally this condition can be satisfied readily.

Thirdly, based on the reduced scheme, a group of equations can be obtained as,

$$\left.\frac{dC_j}{dt}\right|_{\Delta} = \varphi_j(k_{f1}, k_{b1}, k_{f2}, k_{b2}, ..., k_{fm}, k_{bm}, C_1, C_2, ..., C_n),\ (j = 1,2,...,n) \quad \text{..... (1)}$$

$$\left.\frac{dC_j}{dt}\right|_{\nabla} = \psi_j(k_{f1}, k_{b1}, k_{f2}, k_{b2}, ..., k_{fm}, k_{bm}, C_1, C_2, ..., C_n),\ (j = 1,2,...,n) \quad \text{..... (2)}$$

where,

$\left.\frac{dC_j}{dt}\right|_{\Delta}$ - the j-th species production rate, mol/cm^3/s,

$\left.\frac{dC_j}{dt}\right|_{\nabla}$ - the j-th species consumption rate, mol/cm^3/s,

C_j - the j-th species concentration, mol/cm^3,

k_{fi} - the i-th forward reaction rate constant, in units of mol/cm^3, s^{-1},

k_{bi} - the i-th backward reaction rate constant, in units of mol/cm^3, s^{-1},

m - the number of reaction steps,

n - the number of species involved in the reduced scheme.

(The meanings of Δ, ∇, f and b in the following chapters are the same as here.)

In the equations, $\left.\frac{dC_j}{dt}\right|_{\Delta}$, $\left.\frac{dC_j}{dt}\right|_{\nabla}$ and C_j ($j = 1,2,...,n$) are assumed to share the same values in the detailed scheme, respectively. Namely, the species concentrations, the species production and consumption rates in the reduced scheme are assumed to be equal to those of the detailed scheme. This is an important assumption of the method. Therefore (1) and (2) are actually $2n$ independent linear equations with $2m$ unknown variables of k_{fi} and k_{bi} ($i = 1,2,...,m$). In terms of the requirements to the reduced scheme mentioned above, m should be no more than n. So there are two possibilities. If m is equal to n, the solutions about the reaction rate constants can be obtained exactly; if m is less than n, that is, the number of equations is greater than the number of variables, then least-square solutions of the reaction rate constants can be obtained.

Next, the reaction rate constants of the reduced scheme are obtained by solving (1) and (2) under different initial conditions. Then a database with the parameters of initial composition X_0, initial temperature T_0, initial pressure P_0, process temperature T, process pressure P, species concentration C_j during reactions, and reaction rate constants, k_{fi}, k_{bi}, during reactions, is recorded in certain time steps.

Finally, the reaction rate constants, k_{fi}, k_{bi}, are assumed to be polynomial functions of the parameters recorded in the database. Namely,

$$k_{fi} = \xi(X_0, T_0, P_0, T, P, C_1, C_2, ..., C_n), \ (i = 1,2,...,m) \quad \text{..... (3)}$$

$$k_{bi} = \zeta(X_0, T_0, P_0, T, P, C_1, C_2, ..., C_n), \ (i = 1,2,...,m) \quad \text{..... (4)}$$

Because the characteristics of the reaction rates differ largely between the induction zone and the reaction zone, the reaction rate constants are fitted in two phases respectively. The coming section addresses the details of the method using the hydrogen-air system as an example.

3. Numerical Fitting

3.1 Mathematical analysis

A 7-step chemical scheme of hydrogen-air system is chosen here as an example for the detailed scheme. In order to improve the accuracy or to broaden the application range of the reduced models, other more detailed schemes could be chosen without any difficulty.

The chemical equations of the 7-step scheme read as follows [3].

$$\left.\begin{array}{l} H + O_2 \Leftrightarrow OH + O, \\ O + H_2 \Leftrightarrow OH + H, \\ H_2 + OH \Leftrightarrow H_2O + H, \\ 2OH \Leftrightarrow H_2O + O, \\ 2H + M \Leftrightarrow H_2 + M, \\ OH + H + M \Leftrightarrow H_2O + M, \\ 2O + M \Leftrightarrow O_2 + M. \end{array}\right\} \quad \text{..... (5)}$$

The Arrhenius parameters of this 7-step mechanism are shown in Appendix I.

It has been shown that the scheme works well in the range of initial temperatures from 300 K to 3000 K, initial pressures from 0.5 bar to 50 bar [3].

Now steady-state approximations are introduced into the scheme to set up the chemical equations of the reduced scheme. First, if OH is assumed to be in steady-state, the equation system can be simplified like,

$$\left.\begin{array}{l} H_2 + O_2 \Leftrightarrow H_2O + O, \\ 2H_2 + O \Leftrightarrow H_2O + 2H, \\ O_2 + 2H \Leftrightarrow H_2O + O, \\ 2H + M \Leftrightarrow H_2 + M, \\ 2O + M \Leftrightarrow O_2 + M. \end{array}\right\} \quad \text{..... (6)}$$

Similarly, if a steady-state approximation for O is also introduced, a 2-step scheme can be obtained as,

$$\left.\begin{array}{l} 3H_2 + O_2 \Leftrightarrow 2H_2O + 2H, \\ 2H + M \Leftrightarrow H_2 + M. \end{array}\right\} \quad \text{..... (7)}$$

This 2-step reaction mechanism is chosen here as the final reduced scheme. This 2-step model represents the two main phases of a chemical reaction, namely, the build-up of a radical pool (first equation) and the subsequent radical reaction (second equation). If the reaction rates of the two reversible reactions are denoted as $w_{f1}, w_{b1}, w_{f2}, w_{b2}$, and the reaction rate constants, $k_{f1}, k_{b1}, k_{f2}, k_{b2}$, then, based on the two chemical formulas, we have,

$$\left.\begin{array}{l} w_{f1} = k_{f1}[H_2]^3[O_2], \\ w_{b1} = k_{b1}[H_2O]^2[H]^2, \\ w_{f2} = k_{f2}[H]^2[M], \\ w_{b2} = k_{b2}[H_2][M], \end{array}\right\} \quad \text{..... (8)}$$

where $[\bullet]$ denotes species concentrations, and $[M]$ stands for the concentration of third body particles.

Because four species, H_2, H, O_2, H_2O, are involved in the scheme, the following eight kinetic equations can be obtained,

$$\left.\begin{array}{ll} \left.\dfrac{d[H_2]}{dt}\right|_{\nabla} = 3w_{f1} + w_{b2}, & \left.\dfrac{d[H_2]}{dt}\right|_{\Delta} = 3w_{b1} + w_{f2}, \\ \left.\dfrac{d[H]}{dt}\right|_{\nabla} = 2w_{b1} + 2w_{f2}, & \left.\dfrac{d[H]}{dt}\right|_{\Delta} = 2w_{f1} + 2w_{b2}, \\ \left.\dfrac{d[O_2]}{dt}\right|_{\nabla} = w_{f1}, & \left.\dfrac{d[O_2]}{dt}\right|_{\Delta} = w_{b1}, \\ \left.\dfrac{d[H_2O]}{dt}\right|_{\nabla} = 2w_{b1}, & \left.\dfrac{d[H_2O]}{dt}\right|_{\Delta} = 2w_{f1}, \end{array}\right\} \quad \text{..... (9)}$$

where $\left.\dfrac{d[\bullet]}{dt}\right|_{\nabla}$ and $\left.\dfrac{d[\bullet]}{dt}\right|_{\Delta}$ stand for species consumption rate and production rate, respectively. Substituting the w_{fj} and w_{bj} ($j = 1,2$) from (8) to (9), a group of equations can be obtained as follows:

$$
\left.
\begin{aligned}
&\left.\frac{d[H_2]}{dt}\right|_{\nabla} = 3k_{f1}[H_2]^3[O_2] + k_{b2}[H_2][M],\\
&\left.\frac{d[H_2]}{dt}\right|_{\Delta} = 3k_{b1}[H_2O]^2[H]^2 + k_{f2}[H]^2[M],\\
&\left.\frac{d[H]}{dt}\right|_{\nabla} = 2k_{b1}[H_2O]^2[H]^2 + 2k_{f2}[H]^2[M],\\
&\left.\frac{d[H]}{dt}\right|_{\Delta} = 2k_{f1}[H_2]^3[O_2] + 2k_{b2}[H_2][M],\\
&\left.\frac{d[O_2]}{dt}\right|_{\nabla} = k_{f1}[H_2]^3[O_2],\\
&\left.\frac{d[O_2]}{dt}\right|_{\Delta} = k_{b1}[H_2O]^2[H]^2,\\
&\left.\frac{d[H_2O]}{dt}\right|_{\nabla} = 2k_{b1}[H_2O]^2[H]^2,\\
&\left.\frac{d[H_2O]}{dt}\right|_{\Delta} = 2k_{f1}[H_2]^3[O_2].
\end{aligned}
\right\} \quad \text{..... (10)}
$$

If $[\bullet]$, $\left.\frac{d[\bullet]}{dt}\right|_{\nabla}$ and $\left.\frac{d[\bullet]}{dt}\right|_{\Delta}$ are known, then (10) is a linear equation system with variables of $k_{f1}, k_{b1}, k_{f2}, k_{b2}$. Here the equation number is greater than variable number, so least-square solutions can be obtained.

For a given initial condition (X_{H_2}, T_0, P_0) and at a given time, the values of $[\bullet]$, $\left.\frac{d[\bullet]}{dt}\right|_{\nabla}$ and $\left.\frac{d[\bullet]}{dt}\right|_{\Delta}$ can be calculated from running the 7-step detailed scheme. Then the solutions of $k_{f1}, k_{b1}, k_{f2}, k_{b2}$ can be obtained by solving the equation system (10). Here, X_{H_2} is defined as the initial molar ratio of hydrogen according to H_2:O_2:N_2= $X_{H_2}:1:3.76$.

The initial parameters of X_{H_2}, T_0, P_0, and the process parameters T, P, $[H_2]$, $[H]$, $[O_2]$, $[H_2O]$ together with the logarithmic values of reaction rate constants, $\log(k_{f1})$, $\log(k_{b1})$, $\log(k_{f2})$, $\log(k_{b2})$, during the chemical reactions are recorded at every time step. The logarithm function is used because the reaction rate constants vary within a very wide range of magnitude, especially during the induction phase. Many of such records were created to form a sufficient database. These data range,

for X_{H_2}, from 0 to 2 with step of $\Delta X_{H_2} = 0.1$,
for T_0, from 300 K to 3000 K with step of $\Delta T_0 = 20$ K,
for P_0, from 0.5 bar to 50 bar with step of $\Delta P_0 = 2$ bar.

The time step could vary in the detailed scheme calculation, within a range from 1×10^{-9} s to 4×10^{-8} s. The choosing of this time step depends on different initial conditions. Normally the higher the temperature, or the higher the pressure is, the faster the reaction and the shorter the time step must be chosen. The size of the total data file is as large as 634 MB.

The next step of the work is to fit the reaction rate constants numerically. The reaction rate constants of the second reaction in (7), k_{f2} and k_{b2} are assumed to obey an Arrhenius law because this reaction, 2H+M⇔H_2+M, is in fact an elementary one. The Arrhenius parameters can be found in the literature (Appendix I). The logarithmic values of k_{f1} and k_{b1}, the reaction rate constants of the first reaction in (7), are denoted as lk_f and lk_b for convenience.

Figure 3.1.1 shows typical profiles of lk_f and lk_b versus time. It is obvious that there exists a certain critical point. Before this point, lk_f and lk_b grow rapidly. This time period is actually the induction phase. lk_f and lk_b change much more moderately after the critical point than during the induction phase, this period corresponds to the reaction phase. Accordingly lk_f and lk_b can be fitted in two sections respectively.

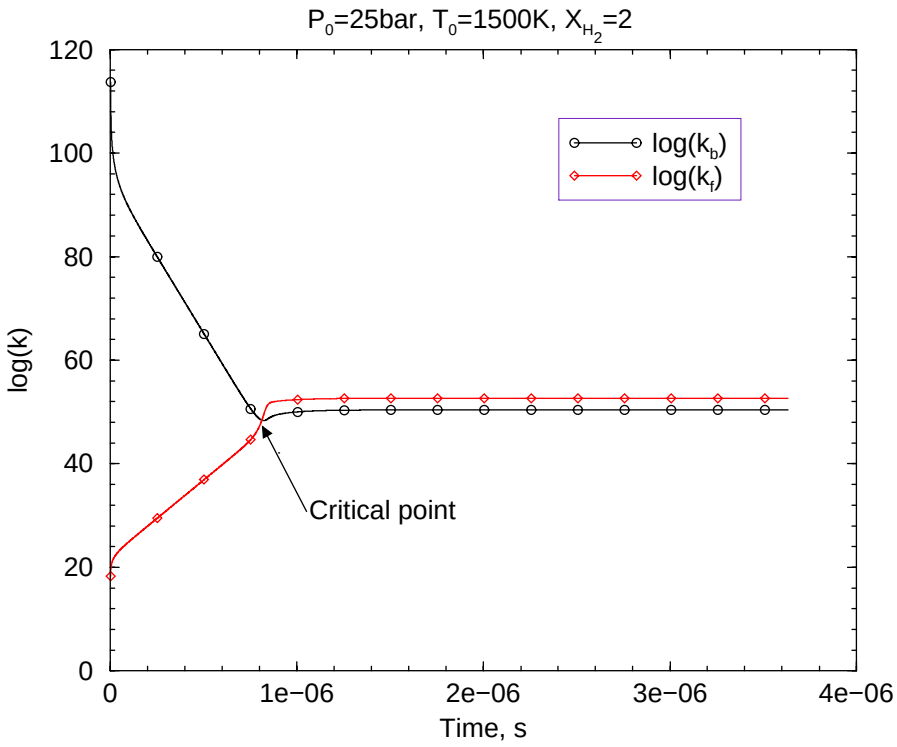

Figure 3.1.1: Typical profiles of forward and backward reaction rate constants, k_f and k_b, for the reaction $3H_2+O_2⇔2H_2O+2H$

3.2 Induction phase

As shown in Figure 3.2.1, lk_f and lk_b are very nearly linear functions of $\log([H])$ before $[H]$ reaches a certain limit, defined as $[H]_r$. In numerical calculations, for all

kinds of initial conditions, $[H]_r$ is turned out to be close to $\exp(-16)$ approximately. This initial stage is actually corresponding to the induction phase, in which the radical pool is built up. Only when the radical H has accumulated to a certain extent, a rapid chemical reactions can take place.

For a given initial condition, lk_j in the induction phase can be assumed to satisfy the relation,

$$lk_j = \mathrm{A}_j \log([H]) + \mathrm{B}_j, \text{ when } [H] < [H]_r,\ j = f \text{ or } b. \quad \text{..... (11)}$$

Figure 3.2.2 shows an example of the curves of lk_j versus $\log([H])$ in different initial conditions. According to the figure, all the lines have only two slopes, +1 or -2, but their interceptions are different. Namely, A_f and A_b in (11) should be equal to +1 and -2, respectively. If B_j is assumed to be functions of initial parameters X_{H_2}, T_0, P_0, then,

$$\left.\begin{aligned} lk_f &= \log([H]) + \mathrm{B}_f(X_{H_2}, T_0, P_0), \\ lk_b &= -2\log([H]) + \mathrm{B}_b(X_{H_2}, T_0, P_0). \end{aligned}\right\} \quad \text{..... (12)}$$

Based on the database obtained from the detailed scheme (mentioned above), for every initial condition, lk_f and lk_b in the induction phase, for which $[H]$ is less than $[H]_r$, are fitted linearly, then the interceptions, B_f and B_b are obtained. (The slopes are indeed equal to +1 or -2, respectively, within a relative error of 0.01%.) Then the initial parameters X_{H_2}, T_0, P_0, together with B_f and B_b form another sub-database in order to determine the expressions of $\mathrm{B}_f(X_{H_2}, T_0, P_0)$ and $\mathrm{B}_b(X_{H_2}, T_0, P_0)$.

B_f and B_b are assumed to have certain identical polynomial terms, where only the corresponding coefficients are different. Based on certain functional characteristics suggested by the sub-database itself and numerical probations, these terms are specified as,

$$\left.\begin{aligned} x_1 &= \log(X_{H_2}), \\ x_2 &= x_1 T_0, \\ x_3 &= \log(P_0), \\ x_4 &= 1, \\ x_5 &= T_0, \\ x_6 &= 2T_0 x_5 - x_4, \\ x_7 &= 2T_0 x_6 - x_5, \\ x_8 &= 2T_0 x_7 - x_6. \end{aligned}\right\} \quad \text{..... (13)}$$

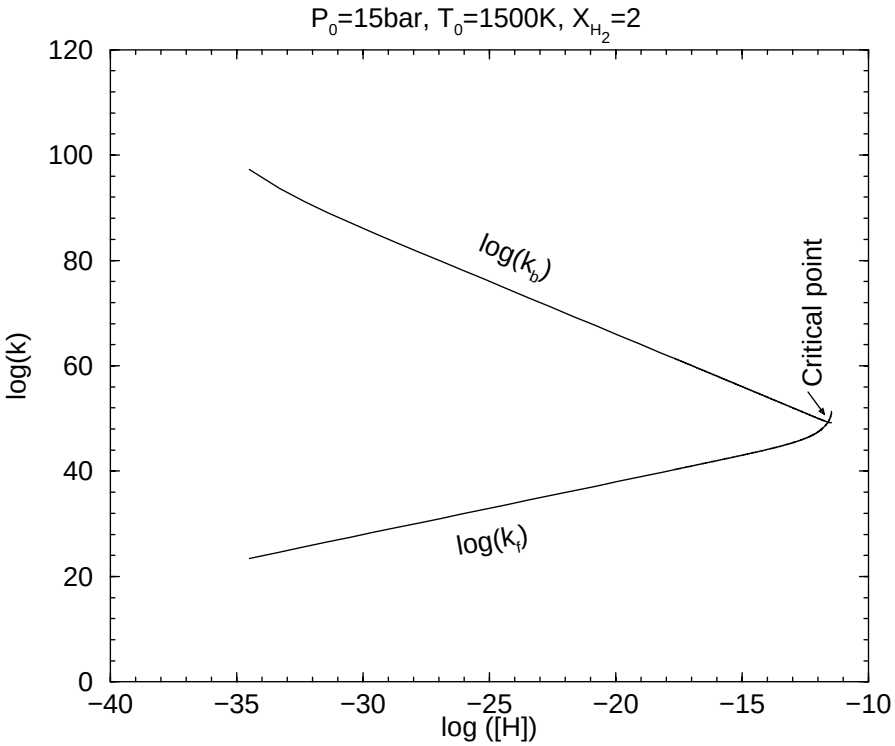

Figure 3.2.1: Typical profiles of $\log(k)$ versus $\log([H])$ for the reaction $3H_2+O_2 \Leftrightarrow 2H_2O+2H$

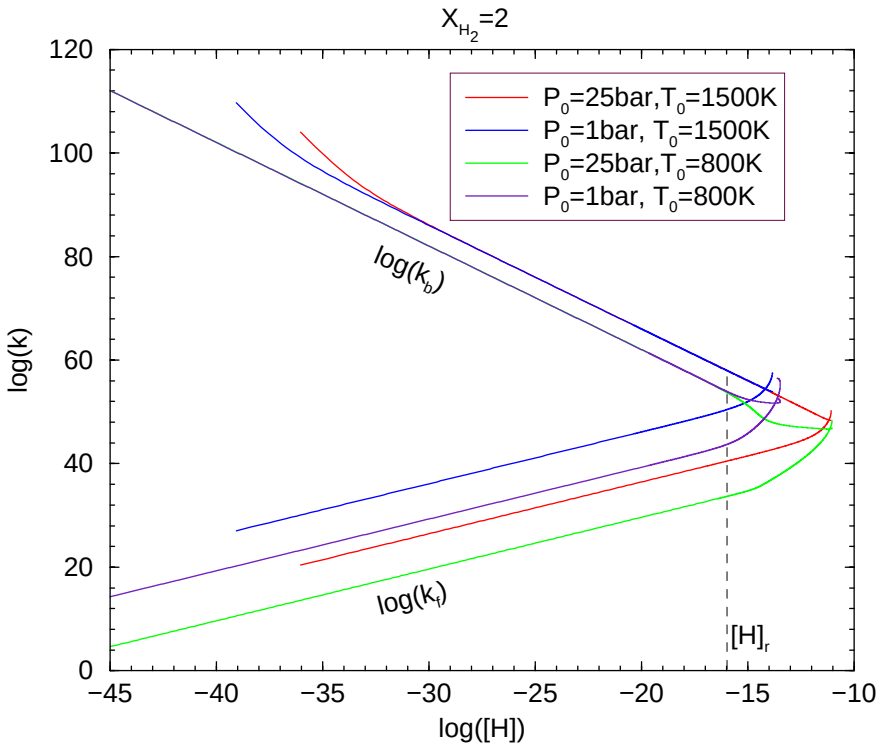

Figure 3.2.2: Profiles of $\log(k)$ versus $\log([H])$ with various P_0 and T_0 for the reaction $3H_2+O_2 \Leftrightarrow 2H_2O+2H$

Then,

$$\left.\begin{aligned}\sum_{i=1}^{8} c_{fi} x_i &= \mathrm{B}_f \ , \\ \sum_{i=1}^{8} c_{bi} x_i &= \mathrm{B}_b \ ,\end{aligned}\right\} \qquad \text{..... (14)}$$

where, c_{ji} denotes the coefficients of the polynomial terms of x_i, ($i = 1,2,...,8$, $j = f$ or b), which is unknown at this moment.

Based on one record in the sub-database, x_i can be determined because X_{H_2}, T_0, P_0 are given, and B_f and B_b are also supplied in the sub-database. Thus an equation with variables of c_{fi} or c_{bi} can be obtained according to (14). The same procedure can be repeated to every record in the sub-database, then two equation systems with variables of c_{fi} and c_{bi} can be obtained respectively. Then the least-square solutions of the two equation systems can be solved. The solutions about c_{fi} and c_{bi} are listed in Appendix II.

For a given initial condition (X_{H_2}, T_0, P_0), we define,

$$\eta = \frac{1}{2}\left(\left|\frac{\mathrm{B}_f - \mathrm{B}_{f0}}{\mathrm{B}_{f0}}\right| + \left|\frac{\mathrm{B}_b - \mathrm{B}_{b0}}{\mathrm{B}_{b0}}\right|\right) \qquad \text{..... (15)}$$

to measure the quality of polynomial fitting, where,

B_j - the computational value from polynomial fitting,
B_{j0} - the original value from the sub-database, $j = f$ or b.

The calculation shows that the mean value of η for all initial conditions is about 0.7%.

Therefore, for the expressions of lk_f and lk_b in the induction phase, the following results have been obtained,

$$\left.\begin{aligned} lk_f &= \log([H]) + \sum_{i=1}^{8} c_{fi} x_i \ , \\ lk_b &= -2\log([H]) + \sum_{i=1}^{8} c_{bi} x_i \ .\end{aligned}\right\} \qquad \text{..... (16)}$$

In realistic applications, the initial values of T_0 and P_0 can be readily substituted by the current values during the induction chemical reactions, T and P, because, during the induction phase, the current values are very close to the initial ones. Numerical tests show that such substitutions add very little error. The model with these process parameters is much more convenient to use, because the COM3D

code only stores the actual variables of the current and the previous time step in each computational cell.

3.3 Reaction phase

The typical temperature dependencies of lk_f and lk_b during the reaction phase under different initial conditions are shown in Figure 3.3.1 and Figure 3.3.2. In this phase, lk_f and lk_b are supposed to be the functions of the initial molar ratio of hydrogen, X_{H_2}, and the process parameters T and P. Although the initial parameters are not stored in the COM3D code, X_{H_2} can be calculated using the process parameters simply according to the conservation law of atomic species. If hydrogen is the only molecular species containing element H in the initial mixture, then X_{H_2} in the reaction process can be calculated using,

$$X_{H_2} = \frac{[H_2] + \frac{1}{2}[H] + [H_2O]}{[N_2]} \cdot 3.76 , \qquad \text{..... (17)}$$

where $[\bullet]$ stands for the species concentrations in the reaction process.

In the light of the features suggested by the data points recorded in the database and numerical probations, the polynomial terms are specified as,

$$\left.\begin{aligned}
y_1 &= \log(X_{H_2}),\\
y_2 &= y_1 P,\\
y_3 &= y_2 P,\\
y_4 &= y_3 P,\\
y_5 &= y_1 T,\\
y_6 &= y_5 T,\\
y_7 &= y_6 T,\\
y_8 &= \log(P),\\
y_9 &= y_8 T,\\
y_{10} &= y_9 T,\\
y_{11} &= y_{10} T,\\
y_{12} &= y_1 y_9,\\
y_{13} &= 1,\\
y_{14} &= \log(T),\\
y_{15} &= 1/T,\\
y_{16} &= \sqrt{T},\\
y_{17} &= y_{15}/T.
\end{aligned}\right\} \qquad \text{..... (18)}$$

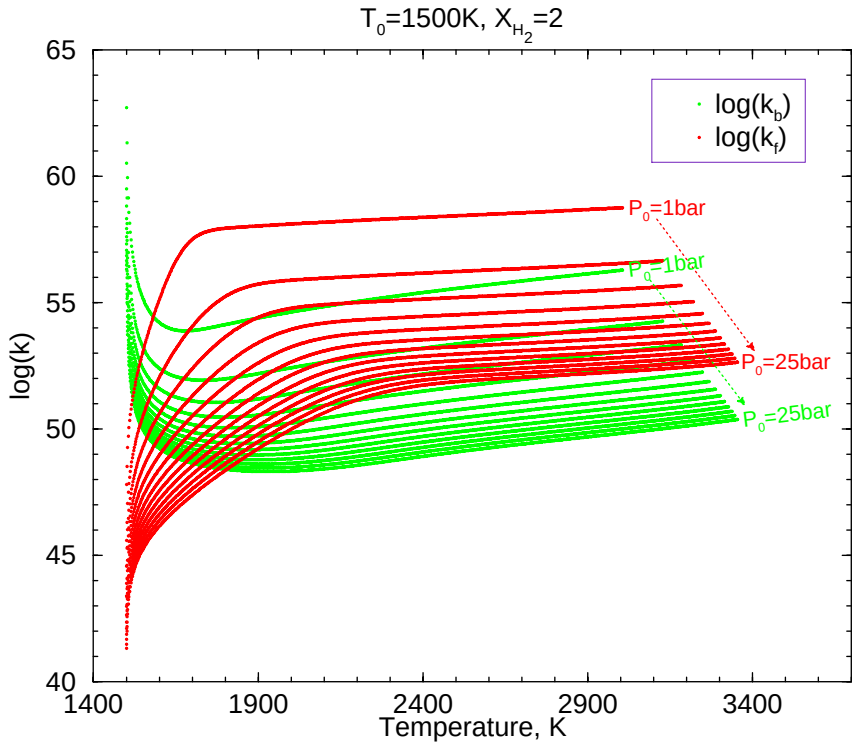

Figure 3.3.1: Temperature dependency of $\log(k)$ for different initial pressure P_0, as calculated from the detailed (7-step) scheme

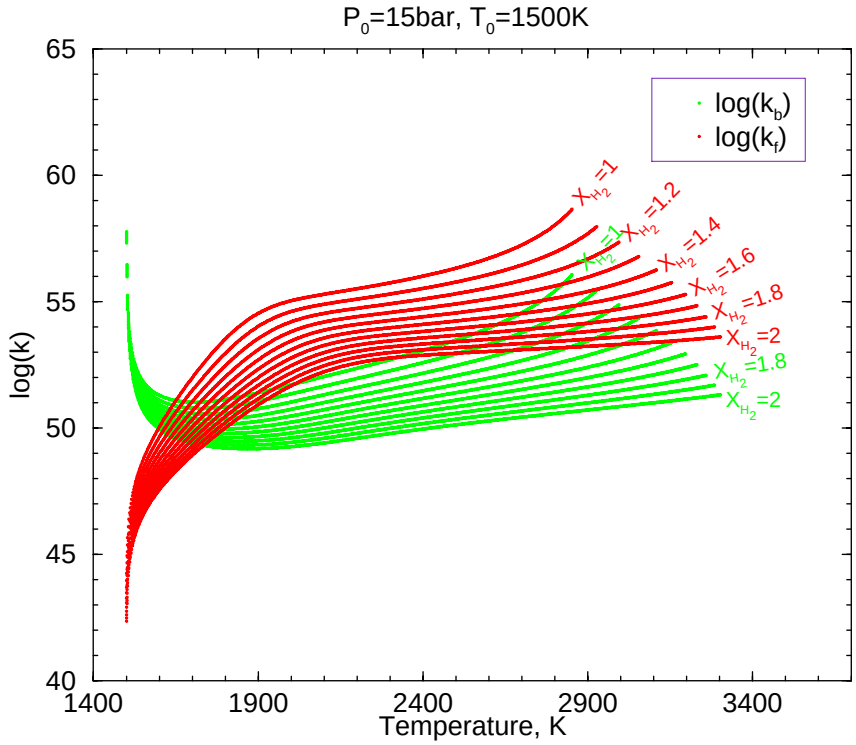

Figure 3.3.2: Temperature dependency of $\log(k)$ for different initial composition X_{H_2}, as calculated from the detailed (7-step) scheme

Then we suppose,

$$\left.\begin{aligned}\sum_{i=1}^{17} d_{fi} y_i &= lk_f ,\\ \sum_{i=1}^{17} d_{bi} y_i &= lk_b .\end{aligned}\right\} \qquad \text{..... (19)}$$

Based on the database obtained from the detailed scheme, for every record in the reaction phase which $[H]$ is greater than $[H]_r$, the terms of y_i can be calculated using X_{H_2}, T and P, lk_f and lk_b are given directly from the database. Then two equation systems about d_{fi} and d_{bi} can be obtained respectively. The least square method is adopted to solve the equation systems. The least square solutions of d_{fi} and d_{bi} are listed in Appendix II.

Similar to the induction phase, a relative error θ is defined as,

$$\theta = \frac{1}{2}\left(\left|\frac{lk_f - lk_{f0}}{lk_{f0}}\right| + \left|\frac{lk_b - lk_{b0}}{lk_{b0}}\right|\right), \qquad \text{..... (20)}$$

where,

lk_j - the value from polynomial fitting,
lk_{j0} - the original value from the database, $j = f$ or b.

Numerical tests show that the mean θ for all points in the reaction phase is about 0.5%.

3.4 Summary

The whole reduced scheme is summarized here. The two steps of the chemical equations are,

$$\left.\begin{aligned}&3H_2 + O_2 \Leftrightarrow 2H_2O + 2H,\\ &2H + M \Leftrightarrow H_2 + M.\end{aligned}\right\} \qquad \text{..... (7)}$$

The formulas to calculate the reaction rate constants are,

$$k_{f_1} = \begin{cases}\exp(\log([H]) + \sum_{i=1}^{8} c_{fi} x_i), & if\ \log([H]) < -16,\\ \exp(\sum_{i=1}^{17} d_{fi} y_i), & if\ \log([H]) \geq -16,\end{cases} \qquad \text{..... (21)}$$

$$k_{b_1} = \begin{cases} \exp(-2\log([H]) + \sum_{i=1}^{8} c_{bi} x_i), & if\ \log([H]) < -16, \\ \exp(\sum_{i=1}^{17} d_{bi} y_i), & if\ \log([H]) \geq -16, \end{cases} \quad \text{..... (22)}$$

$$k_{f_2} = A_{f_2} T^{\beta_{f_2}} \exp(-\frac{E_{f_2}}{RT}), \quad \text{..... (23)}$$

$$k_{b_2} = A_{b_2} T^{\beta_{b_2}} \exp(-\frac{E_{b_2}}{RT}), \quad \text{..... (24)}$$

where x_i and y_i are shown in (13) and (18) respectively, c_{fi}, d_{fi}, c_{bi} and d_{bi} are listed in Appendix II, A_{f_2}, A_{b_2}, β_{f_2}, β_{b_2}, E_{f_2} and E_{b_2} are given in Appendix I (the fifth reaction). Here polynomials with 8 terms and 17 terms are adopted respectively. If a more precise solution is needed, more terms can in principle be added into the polynomials, however the quantity of calculation would be increased.

The range of application of the reduced model developed here is,

$$\left.\begin{array}{l} 0 \leq X_{H_2} \leq 2, \\ 300\ \text{K} \leq T \leq 3000\ \text{K}, \\ 0.5\ \text{bar} \leq P \leq 50\ \text{bar}. \end{array}\right\} \quad \text{..... (25)}$$

4. Comparison between reduced and detailed schemes

The comparison between the reduced scheme and the detailed scheme is made for a zero-dimensional adiabatic homogeneous closed system. The case with the initial conditions $X_{H_2} = 2$, $P_0 = 25$ bar and $T_0 = 1500$ K, is shown as an example. Figure 4.1 shows the species molar concentration profiles versus time with the reduced model. Figure 4.2 shows the corresponding results of the detailed model. It is clear that the primary characters of the profiles are very similar in the two models. As key parameters of the chemical process, the induction delay time and the thickness of reaction zone are very close to each other between the simplified model and the detailed model.

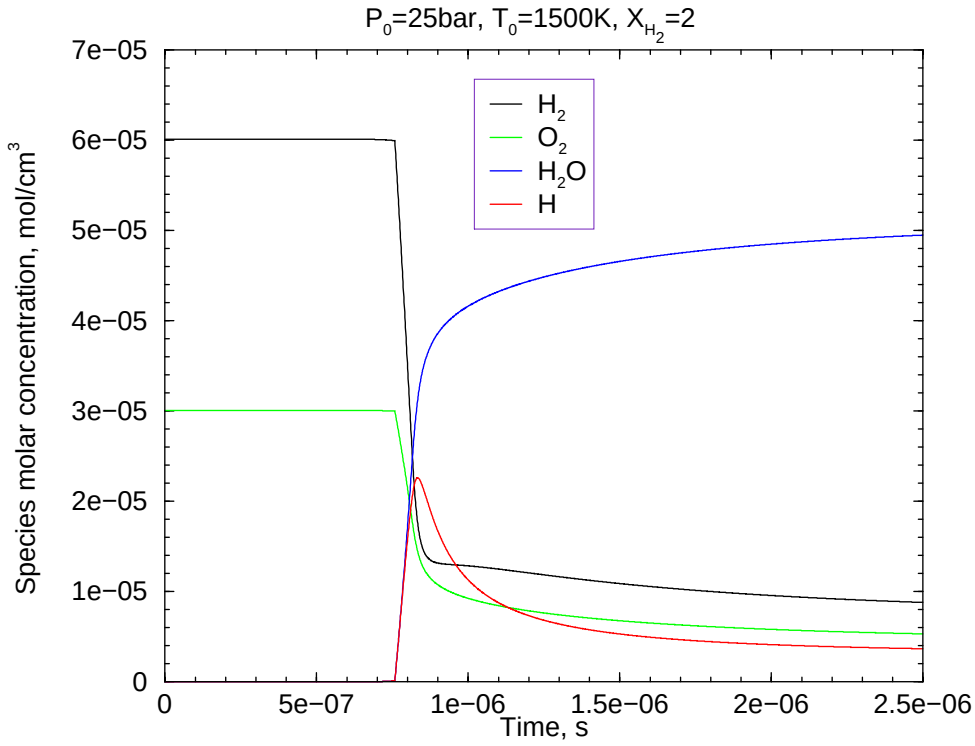

Figure 4.1: An application example of the simplified scheme

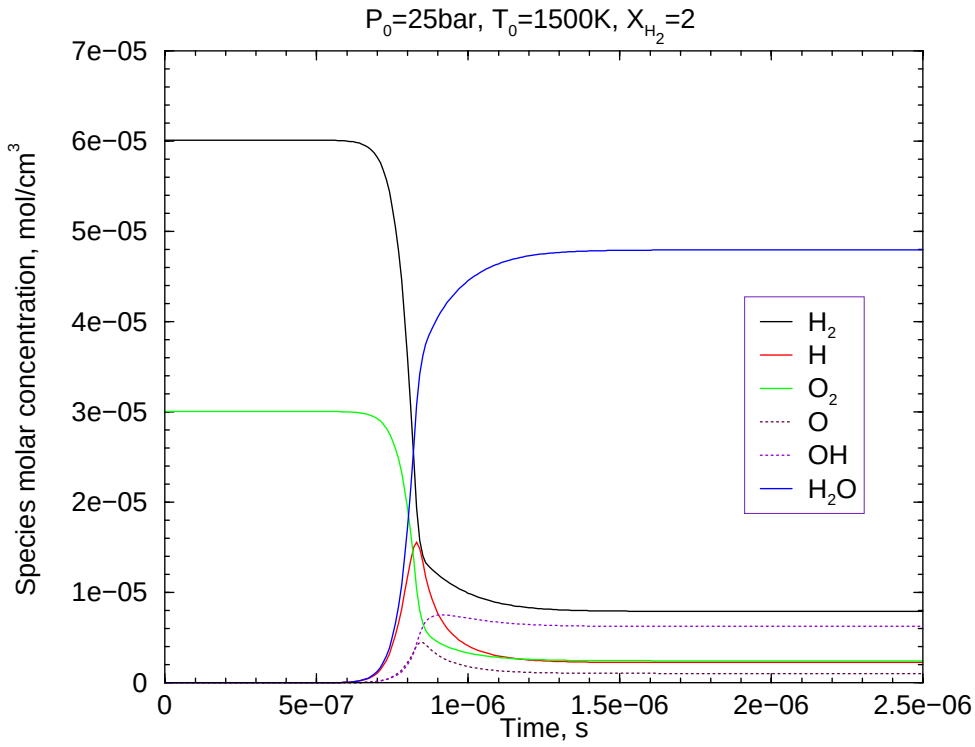

Figure 4.2: An application example of the detailed scheme

More generally, the two key performance indices of a chemical model, the induction delay time and the reaction zone thickness of the two models are compared under different initial conditions.

As starting point of the induction delay time we select the mixture in its initial state, and the end point as the moment when $[H_2]$ is decreased by 1% of the original concentration, $[H_2]_0$. Namely, the induction time is defined as,

$$\tau_{in} \equiv t\,|_{[H_2]=0.99[H_2]_0} - t\,|_{[H_2]=[H_2]_0} . \qquad \text{..... (26)}$$

At a given initial pressure P_0, the logarithmic plot of the induction time increases with $1/T_0$ almost linearly. Figure 4.3 shows the comparison for $P_0 = 1$ bar. Similarly, the cases for 15 bar and 25 bar are shown in Figure 4.4 and Figure 4.5, respectively. In another view, the relation between the induction time and the initial pressure is also shown at a given initial temperature. The cases of $T_0 = 800$ K and $T_0 = 1500$ K are shown as examples in Figure 4.6 and Figure 4.7, respectively. The figures show clearly that the simplified scheme can simulate the induction time of the detailed scheme over 3 orders of magnitude.

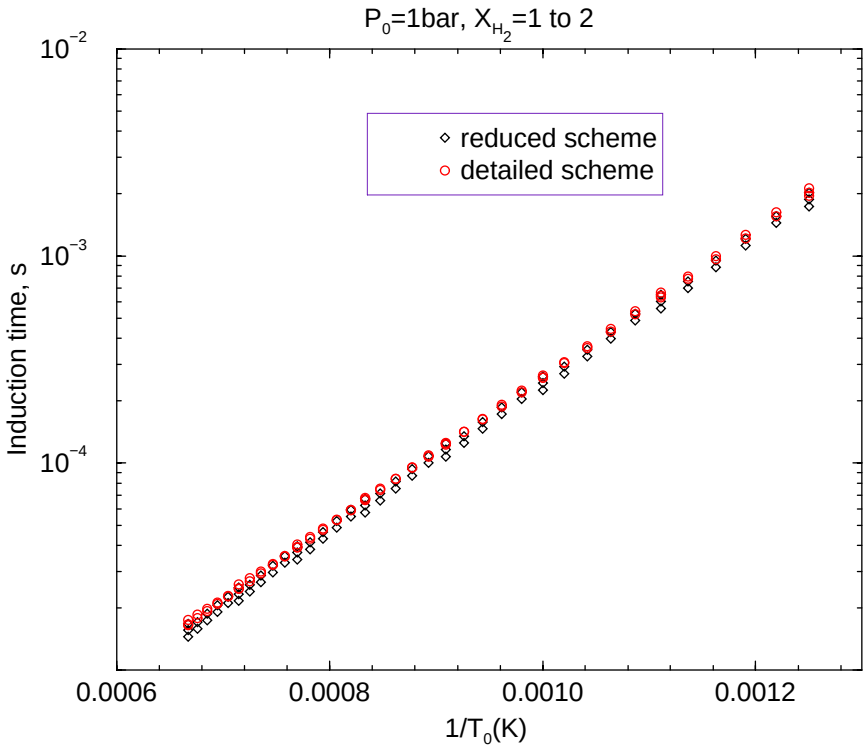

Figure 4.3: Comparison of induction times versus T_0 for $P_0 = 1$ bar

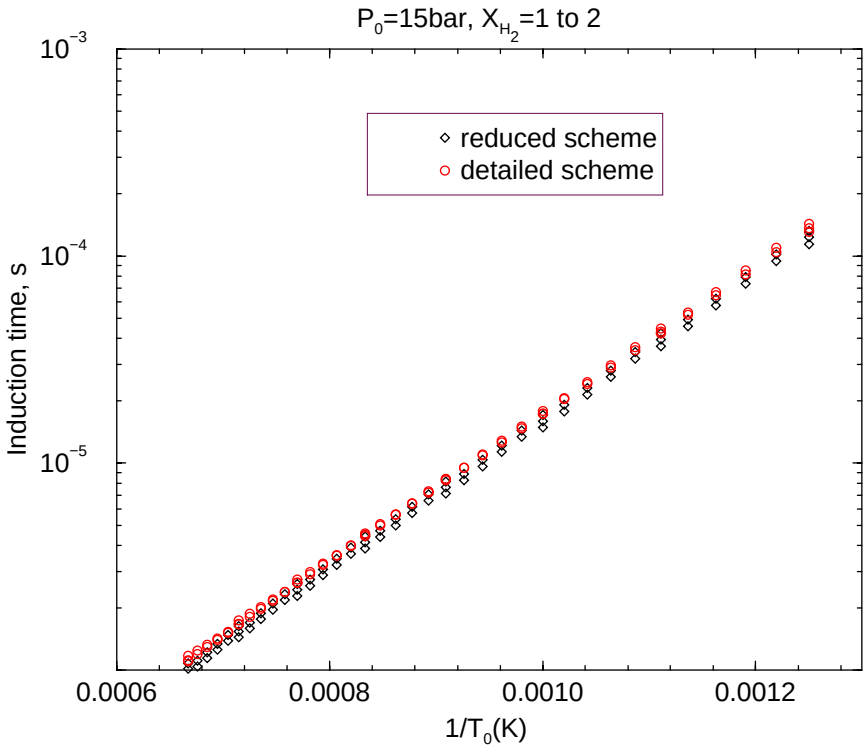

Figure 4.4: Comparison of induction times versus T_0 for $P_0 = 15$ bar

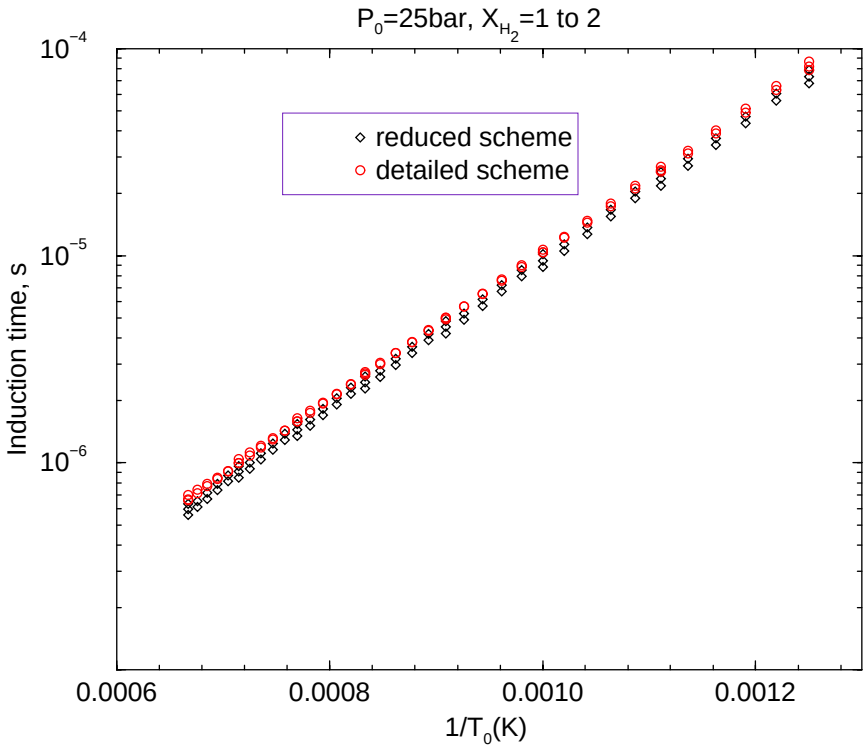

Figure 4.5: Comparison of induction times versus T_0 for $P_0 = 25$ bar

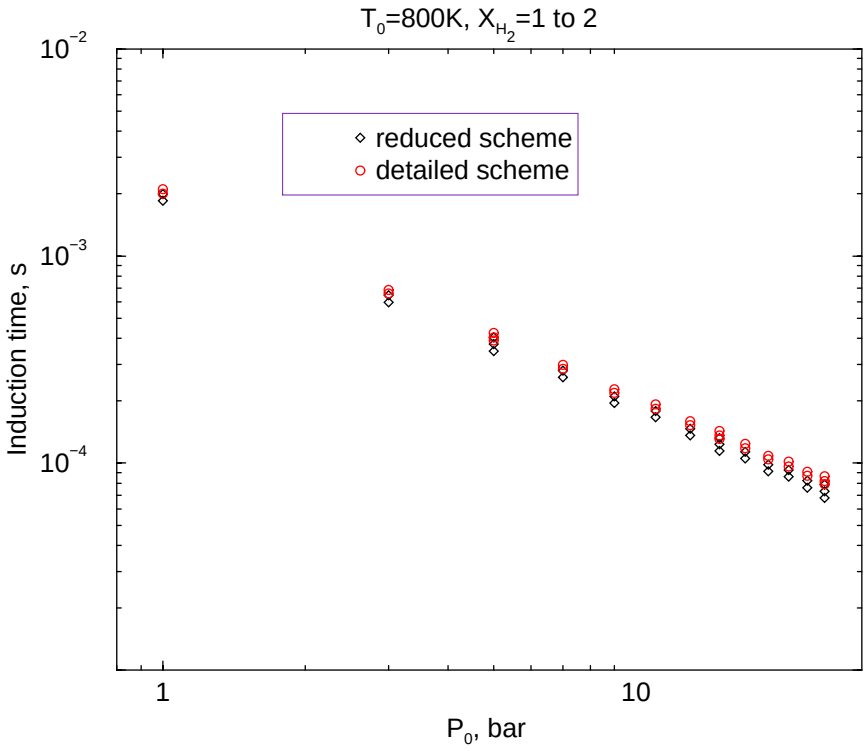

Figure 4.6: Comparison of induction times versus P_0 for $T_0 = 800$ K

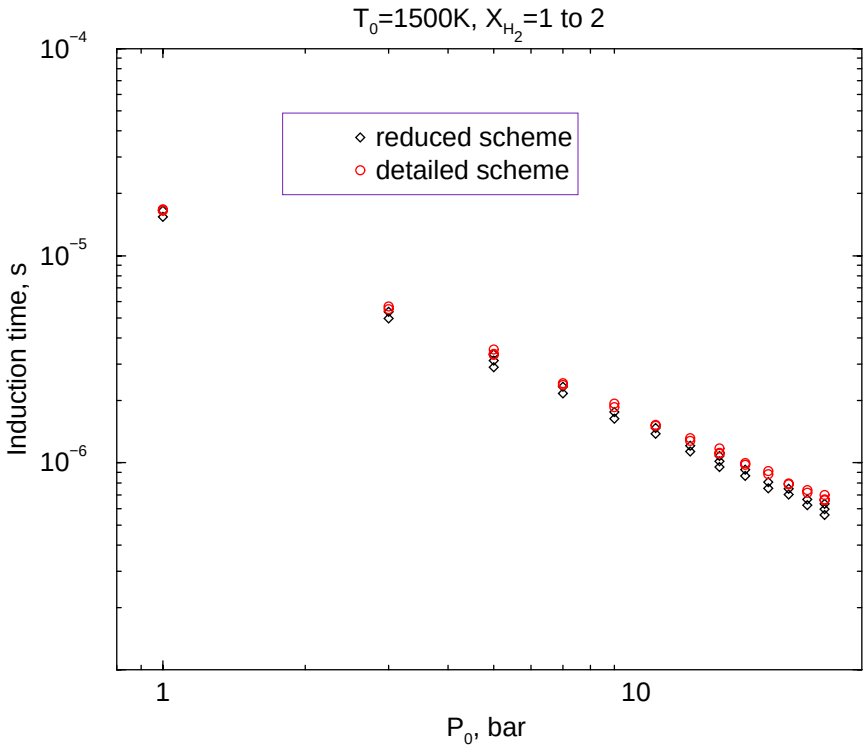

Figure 4.7: Comparison of induction times versus P_0 for $T_0 = 1500$ K

As shown in Figure 4.1 or Figure 4.2, the time-dependent H concentration always reaches a peak value. We define here the reaction time as the full width at half maximum of the H concentration, namely,

$$\tau_{re} \equiv \Delta t \,|_{[H]=0.5[H]_{\max}} . \qquad \text{..... (27)}$$

The relations between the reaction time and the initial pressure are shown in Figures 4.8 to 4.10 for different initial conditions. The plots show that the reaction time of the reduced scheme in the chosen definition is about a factor of 3 larger than that of the detailed scheme over a total range of three orders of magnitude (10^{-7} to 10^{-4} s).

In summary, the induction time and the reaction time of the reduced model agree satisfactorily with the detailed (7-step) scheme. The deviations between the reduced scheme and the detailed scheme are comparable to the current differences between various detailed H_2-O_2 reaction mechanisms found in the literatures. Therefore no further attempt was made to improve the agreement between the reduced and detailed models by using more polynomial terms in the fitting procedure, which on the other hand would increase the computational effort within a COM3D chemistry calculation.

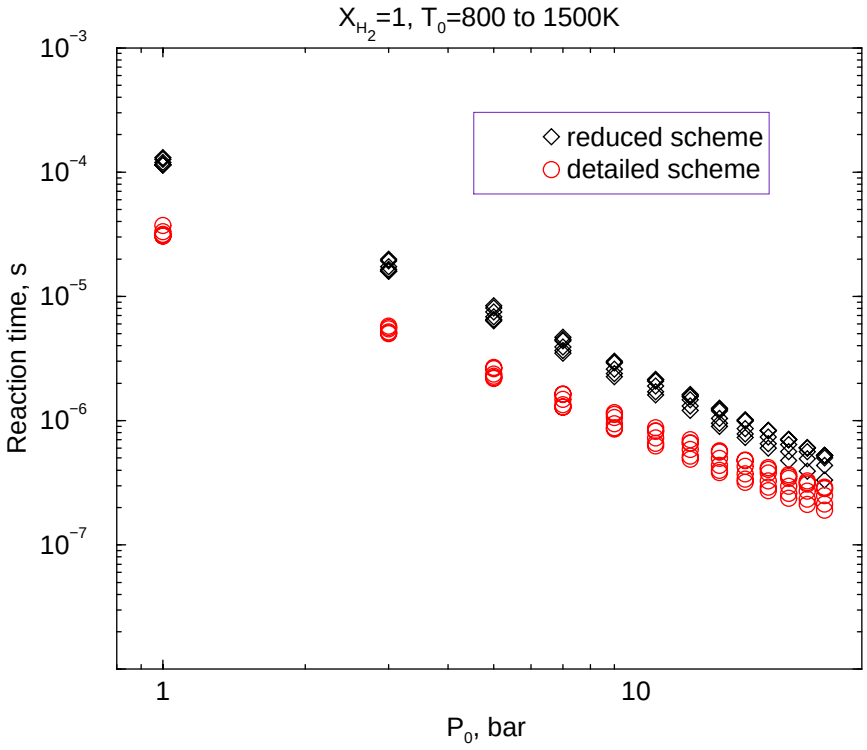

Figure 4.8: Comparison of reaction times versus P_0 for $X_{H_2} = 1$

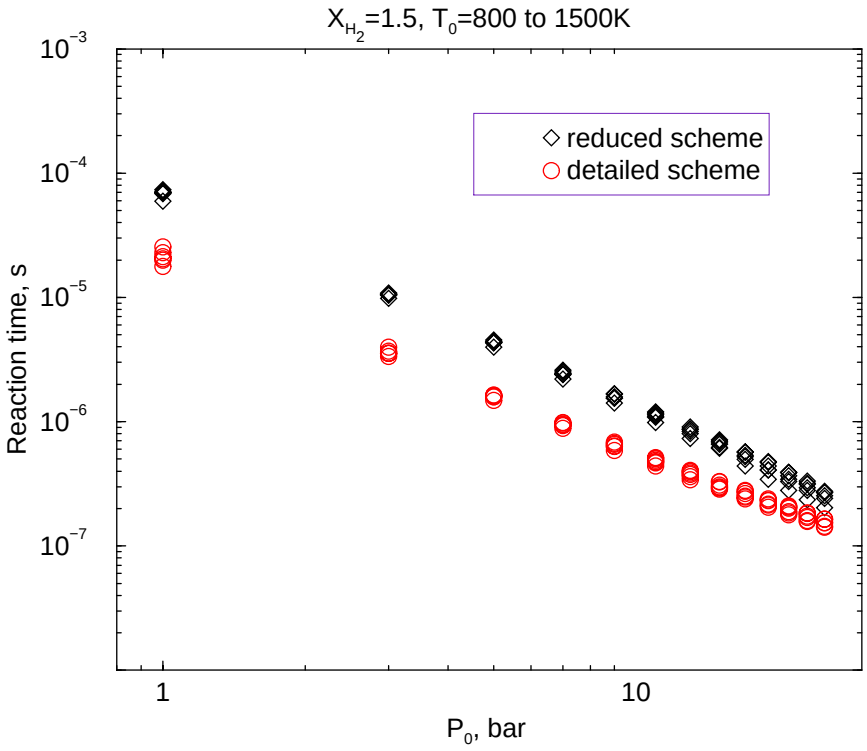

Figure 4.9: Comparison of reaction times versus P_0 for $X_{H_2} = 1.5$

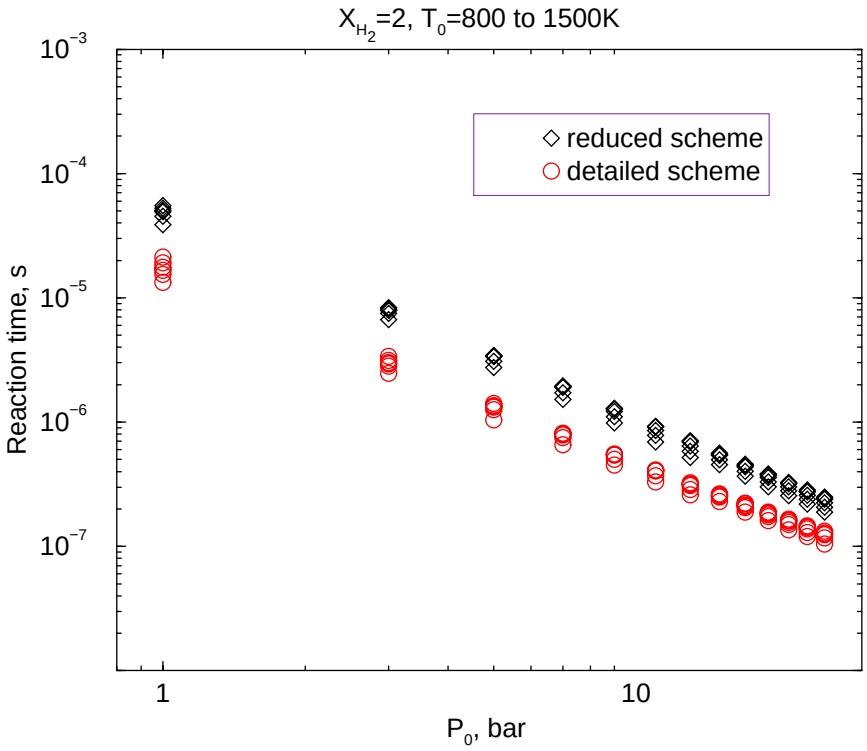

Figure 4.10: Comparison of reaction times versus P_0 for $X_{H_2} = 2$

5. COM3D implementation

Prior to implementation of the new reduced 2-step model, the COM3D code was generalized from the original four components (H_2, O_2, N_2 and H_2O) to an arbitrary number of reactive components in order to allow the introduction of the radical H.

5.1 The modified chemical calculation module

The time step of the chemical calculation is different from that of the flow calculation. Especially in the acute reaction phase, the chemical time step is much smaller than the flow calculation time step. Therefore, one iteration of the flow calculation is corresponding to several or several dozens of iterations of the chemical calculation. The schematic structure of the chemical module for the COM3D code is shown in Figure 5.1.1.

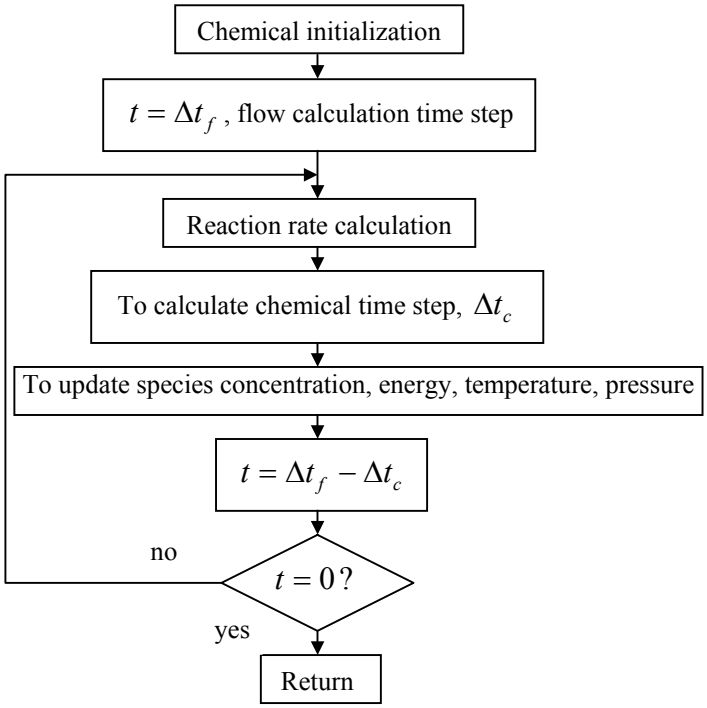

Figure 5.1.1: Flow chart of the new chemical module for COM3D

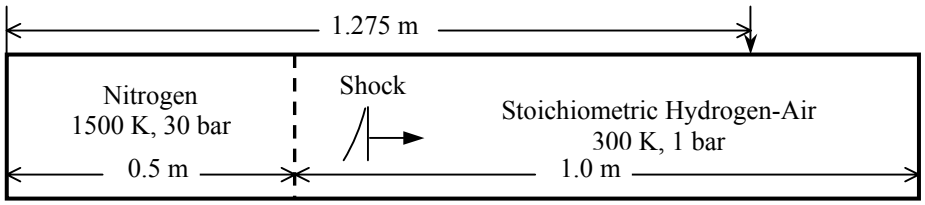

Figure 5.2.1: Configuration of the shock tube for sensitivity analysis of the new reduced chemistry module for COM3D

5.2 Sensitivity analysis

The sensitivity of the chemical model on the geometrical cell size has been analyzed with the updated COM3D code by means of a one-dimensional test problem. The geometry is assumed as a one-dimensional shock tube consisting of two sections. The high pressure section is filled with nitrogen at high temperature and the low pressure section contains stoichiometric hydrogen-air with room temperature. The schematic plot of the tube is shown in Figure 5.2.1. When the shock wave arrives at the point of 1.275 m, the species concentration profiles, the pressure and temperature are recorded. The same problem has been calculated with different cell sizes of 1 mm, 2.5 mm and 5 mm. The calculation results are shown in Figure 5.2.2, 5.2.3 and 5.2.4. These self-explaining pictures obviously show that the primary behavior of the mixture is well duplicated in cases of different cell sizes.

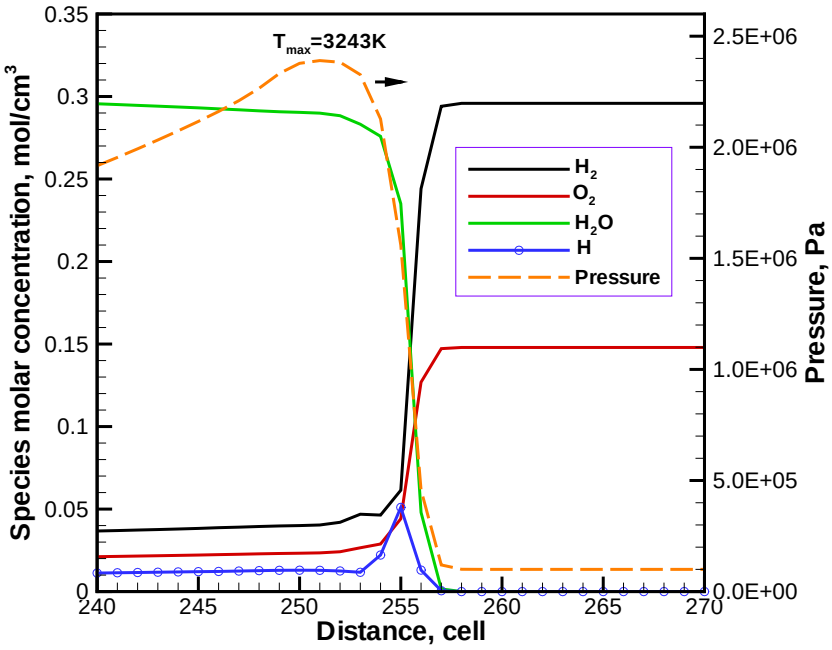

Figure 5.2.2: Concentration profiles of the test case with a cell size of 5 mm

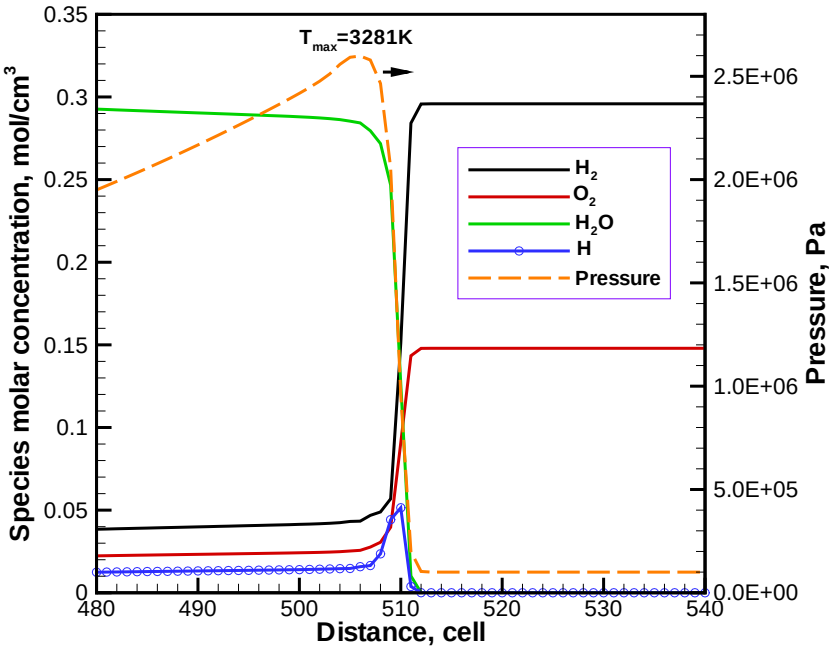

Figure 5.2.3: Concentration profiles of the test case with a cell size of 2.5 mm

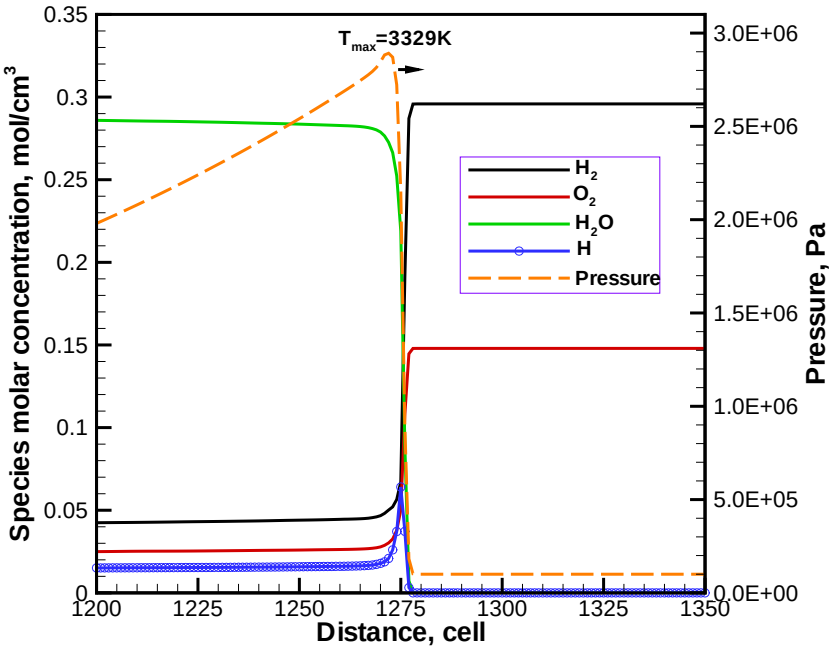

Figure 5.2.4: Concentration profiles of the test case with a cell size of 1 mm

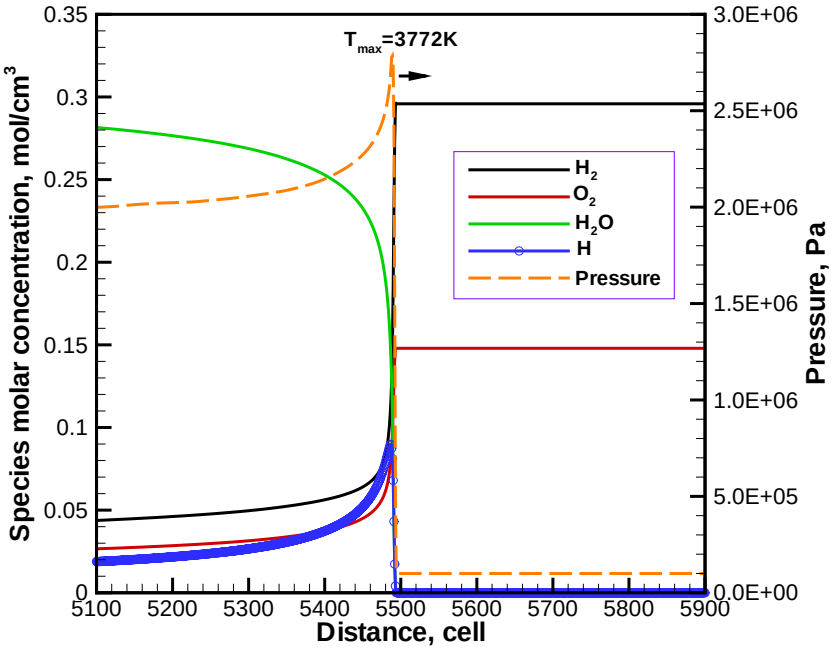

Figure 5.2.5: Concentration profiles of the test case with a cell size of 0.01 mm

A cell size of 0.01 mm was used for a six centimeter long small tube filled with stoichiometric hydrogen-air mixture at 1 bar, 300 K. The mixture is ignited from the left end by a hot spot at 50 bar, 3000 K. The species concentration profiles and the pressure profile are recorded in Figure 5.2.5 while the pressure shock goes through the point of about 5.5 cm. It is clear that the finer grids allows a more precise calculation of the concentration profiles.

The sensitivity analysis shows that the chemical model works well with the cell sizes below about 5 mm. In large scale calculations, a coarse grid trends to be adopted if the problem of CPU time is considered. Numerical calculation shows the cell size of 5 mm is completely applicable.

5.3 Running performance

The time efficiency of the COM3D code was compared between a one-step chemistry model and the new reduced 2-step model for the geometry of a real tube with a wedge-shaped reflector (Figure 6.1.1). The high pressure section is filled with helium at 400 K and 10 bar, the low pressure section is 26% hydrogen in air at 400 K and 1 bar. The problem was run in exactly the same hardware configuration, the same software and running environment, and the same initial condition. For example, after 1500 iterations have been finished, in both cases detonation occurs and the shock wave reaches the same place after detonation. It took 149 minutes CPU time for the one-step scheme, and 151 minutes for the 2-step scheme. Thus, in total, the amount of calculation with the 2-step scheme is only 1.3% more than that of the one-step scheme. However, during the process of calculation, the time index of the 2-step scheme can reach 425 mks/node/step, and 328 mks/node/step for the one-step

scheme. The former is 23% greater than the latter, but this was the worst case observed throughout the whole calculation.

This and other test calculations have demonstrated that the goal to develop a fast running yet precise enough reduced chemistry model for the COM3D code could be achieved by the use of suitable polynomial expressions for the dominant reaction rate constants.

6. Application

6.1 Experiments

In order to verify the updated COM3D code with the reduced chemical model, experiments have been performed in a special shock tube facility [14]. Eight of the experiments are presented here. The geometry of the shock tube is shown in Figure 6.1.1 schematically.

Pressure transducers and photodiodes are installed along the tube. The positions of the gauges are listed in Table 1. The starting point of the distance is the flat, left end of the tube.

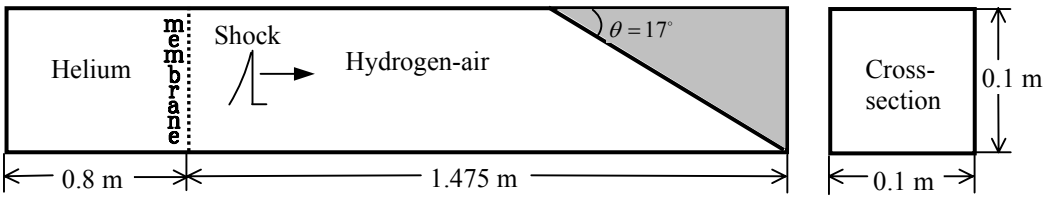

Figure 6.1.1: Geometry of the shock tube

Table 1: Positions of the measurement gauges

Distance, m	0.2	0.4	0.6	0.94	1.14	1.34	1.54	1.74	1.94	2.14
Pressure transducer	√†	√	√	√	√	√	√	√	√	√
Photodiode				√	√	√	√	√	√	√

† √ means being installed.

Table 2: Experimental configurations and results

(Atmosphere temperature is 288K.)

Experiment	% H_2 in air	High pressure, bar †a	Low pressure, bar	Incident wave speed, m/s †b mean (min, max)	Incident wave Mach number mean (min, max)	Reflected wave speed, m/s †c mean (min, max)	Flame speed, m/s †d mean (min, max)	DDT
R0601_15	26	4.6	0.856	626 (619,630)	1.601 (1.583,1.611)	1749 (1639,1923)	1604 (1471,1852)	Yes
R0601_16	26	3.9	0.865	602 (596,609)	1.540 (1.524,1.558)	683 (595,787)	444 (333,769)	No
R0601_17	26	4.2	0.805	641 (632,649)	1.639 (1.616,1.660)	1709 (1669,1764)	1709 (1515,1942)	Yes
R0601_19	26	4.7	0.906	643 (639,647)	1.645 (1.634,1.655)	704 (597,990)	664 (457,976)	No
R0601_20	26	3.8	0.803	610 (603,617)	1.560 (1.542,1.578)	629 (563,803)	492 (298,794)	No
R0601_21	26	4.1	0.861	614 (612,615)	1.570 (1.565,1.573)	690 (581,952)	644 (442,909)	No
R0601_22	26	4.2	0.908	627 (623,633)	1.604 (1.593,1.620)	694 (585,971)	586 (410,806)	No
R0601_23	26	4.7	1.006	595 (592,600)	1.522 (1.514,1.535)	623 (568,727)	536 (407,658)	No

†a: ± 0.2 bar.

†b: being associated to the pressure transducers at the positions of 1.34m, 1.54m, 1.74m, 1.94m.

†c: being associated to the pressure transducers at the positions of 1.54m, 1.74m, 1.94m, 2.14m.

†d: being associated to the photodiodes at the positions of 1.54m, 1.74m, 1.94m, 2.14m.

The experimental configurations and the main results are listed in Table 2.

As a typical detonation case, the measured pressure and light signals of the experiment R0601_15 are shown in Figure 6.1.2. As shown, the incoming shock wave enters the wedge space with a speed of 626 m/s. While the shock arrives in the corner, a strong ignition happens and energy is emitted from the chemical reaction to accelerate the reflected shock wave. As shown, the reflected shock wave speed reaches up to 1749 m/s, which is a typical theoretical velocity of detonation wave in hydrogen-air mixture propagating against the incoming particle velocity (from left). Obviously deflagration-to-detonation-transition (DDT) occurs in the experiment. It can be seen from Figure 6.1.2 that the strong ignition results in a close coupling between the pressure shock, measured by the pressure transducers, and the flame front, measured by photodiodes. DDT also leads to a relatively high system pressure and temperature.

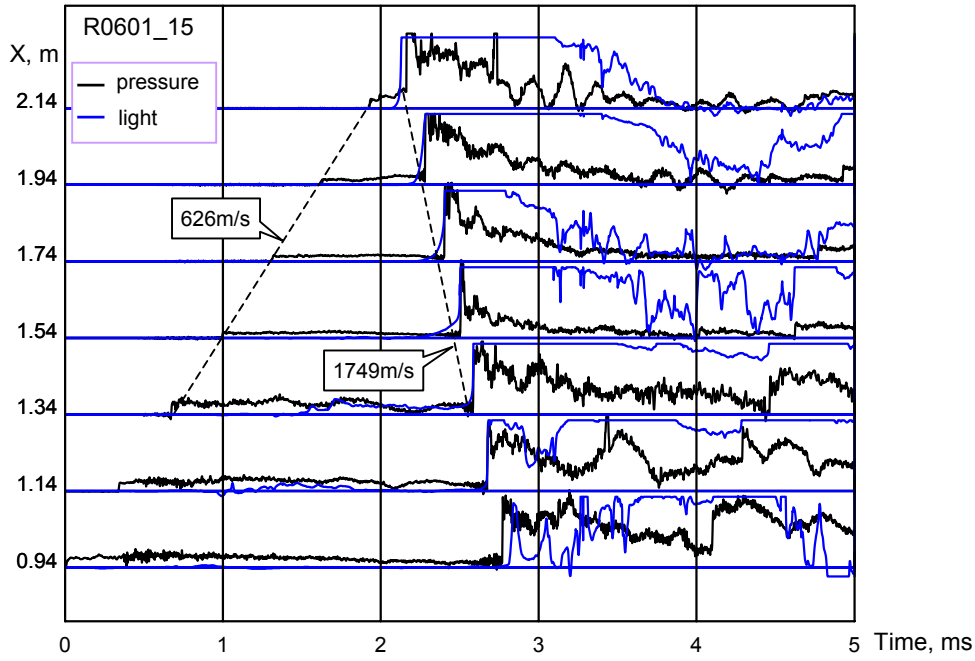

Figure 6.1.2: X-t diagram of the experiment R0601_15, which is an example for DDT

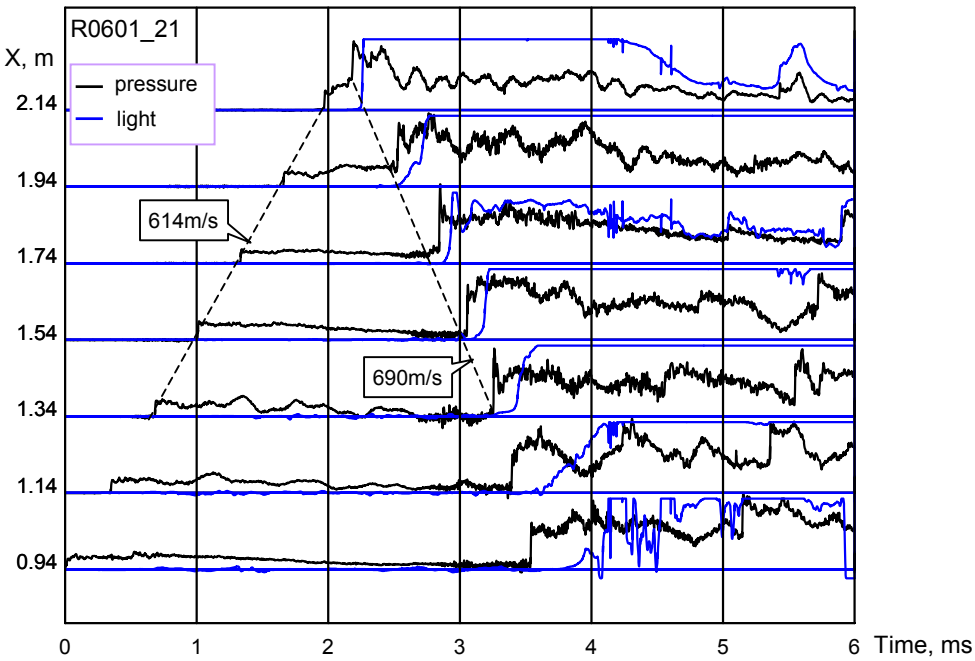

Figure 6.1.3: X-t diagram of the experiment R0601_21, which is an example for mild ignition without DDT

Experiment R0601_21 is selected as an example to show a week ignition case. The experimental record is shown in Figure 6.1.3. In this case, the Mach number of the incoming shock wave is smaller, and the pressure shock is not strong enough to ignite the mixture rapidly. The mild ignition in the wedge does not result in DDT, but is characterized by a decoupled flame front and pressure shock. Lower system pressure and temperature are generated in this case.

The Mach number of the incident shock wave is a governing parameter to determine if DDT happens or not in a given chemical mixture and focusing geometry. Figure 6.1.4 summarizes the experimental points in the plane of reflected wave speed versus Mach number of the incident shock. Error bars for the measured wave speed and the Mach number are also shown. According to the figure, there is a gap between the detonation zone and that without DDT. This gap represents a transition zone. Generally, when the incident shock Mach number is small DDT can not happen; when the Mach number is great DDT will happen in the facility. However, in the transition zone, both week ignition and strong ignition could happen depending on stochastic processes. In this case, very tiny factors could influence the behavior of the mixture, for example, the way of membrane breaking and so on. Unfortunately the experimental set-up did not allow to produce Mach numbers above 1.65, without various disturbances in the pressure transducer data from the shocks traveling in the tube walls.

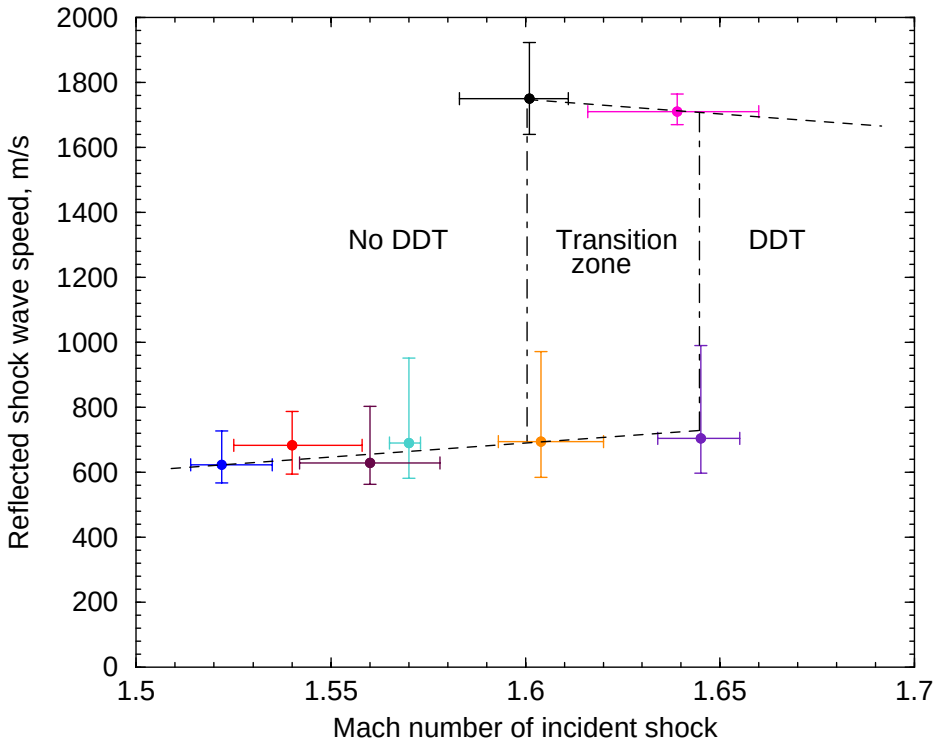

Figure 6.1.4: Experimental diagram of incident shock Mach number versus reflected wave speed

6.2 Calculations

The COM3D code with the new reduced 2-step chemical model was used to simulate the experiments in two dimensions. Eight test calculations have been done according to the geometric configurations and initial conditions of the experiments listed in Table 2. In the calculations, a cell size of 5 mm was used, the Courant number was about 0.9. The computational results are shown in Table 3.

Table 3: Computational results

(Initial temperature is 288K.)

Calculation	% H_2 in air	High pressure, bar	Low pressure, bar	Incident wave speed, m/s †a	Incident wave Mach number	Reflected wave speed, m/s †b	DDT
R0601_15	26	4.5	0.856	626	1.601	1764	Yes
R0601_16	26	3.9	0.865	601	1.537	606	No
R0601_17	26	4.2	0.805	641	1.639	1761	Yes
R0601_19	26	5.2	0.906	643	1.645	1763	Yes
R0601_20	26	3.8	0.803	610	1.560	624	No
R0601_21	26	4.1	0.861	614	1.570	627	No
R0601_22	26	4.7	0.908	628	1.606	1762	Yes
R0601_23	26	4.4	1.006	595	1.522	600	No

†a: being associated to the pressure gauges at the positions of 1.34m, 1.54m, 1.74m, 1.94m.

†b: being associated to the pressure gauges at the positions of 1.54m, 1.74m, 1.94m, 2.14m.

Because the measurement of the high pressure in the experiments was not very reliable in some tests, the high pressure value in the calculation was adjusted in order to obtain nearly the same incident shock wave speed as that measured in the experiments. For example, in the case of test R0601_19, if the high pressure is assumed as the measured value of 4.7 bar, the calculated incident shock wave speed will be 625 m/s, which is lower than the measured speed of 643 m/s in the experiment. In order to create a shock speed of 643 m/s exactly, the high pressure was determined as 5.2 bar by the numerical tests. This computational result of COM3D concerning the relation between the high pressure and the incident shock speed was confirmed by comparison to the BOB code, another three-dimensional combustion code.

The calculated X-t diagram for the case of test R0601_15 is shown in Figure 6.2.1, as an example for a detonation case. The Mach number of the incident shock is 1.601, the same as that in the experiment. In the space of the wedge, high pressures and temperatures are generated, which are the direct factors to ignite the mixture rapidly. Strong detonation causes the shock wave to propagate back with a high velocity of 1764 m/s. The corresponding experimental value is 1749 m/s.

Figure 6.2.2 shows a typical case without DDT, which is the computational result for the case of test R0601_21. It can be seen that a relatively low pressure peak develops, which is not strong enough to ignite the mixture rapidly because the incident shock has only a relatively low Mach number of 1.570.

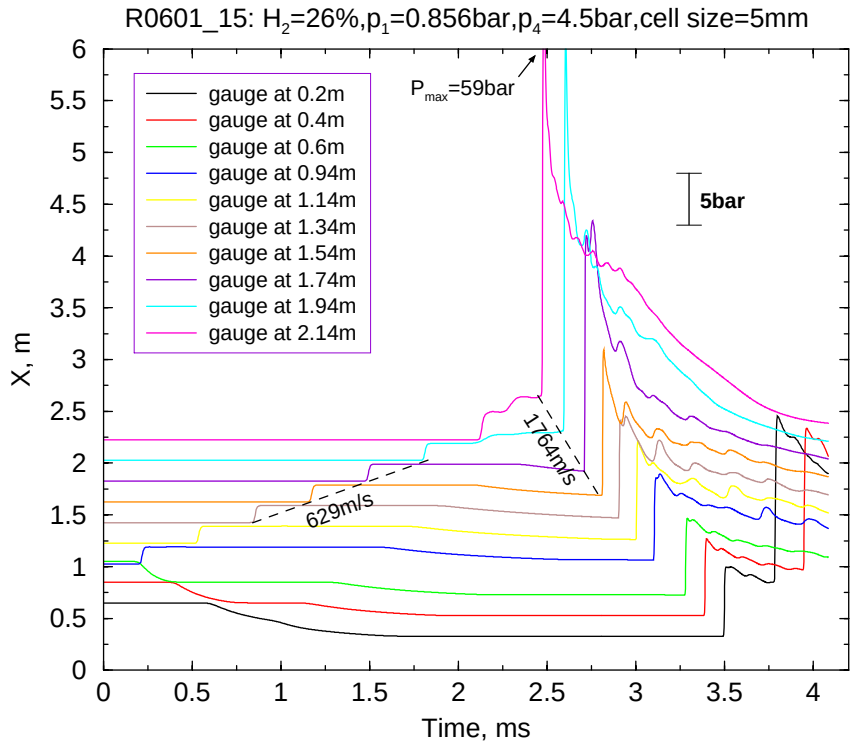

Figure 6.2.1: Calculated X-t diagram of R0601_15, as an example for DDT

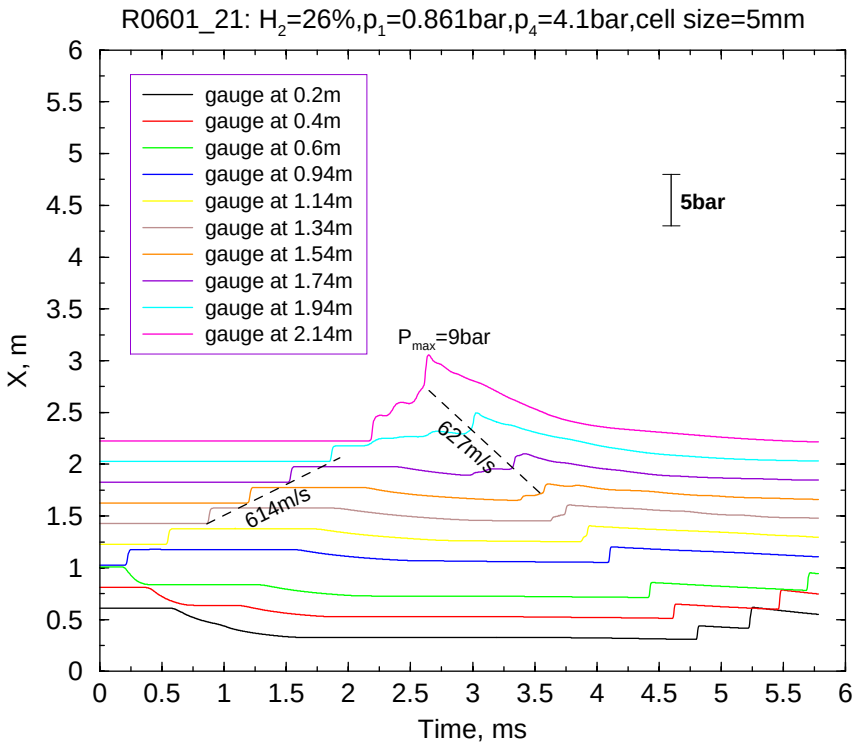

Figure 6.2.2: Calculated X-t diagram of R0601_21, as an example without DDT

The calculated points are drawn in Figure 6.2.3 as a diagram of reflected wave speed versus Mach number of the incident shock. According to the figure, if the Mach number of the incident shock is greater than 1.6, DDT will happen; if it is below 1.57, the model calculations predict only a weak ignition (deflagration).

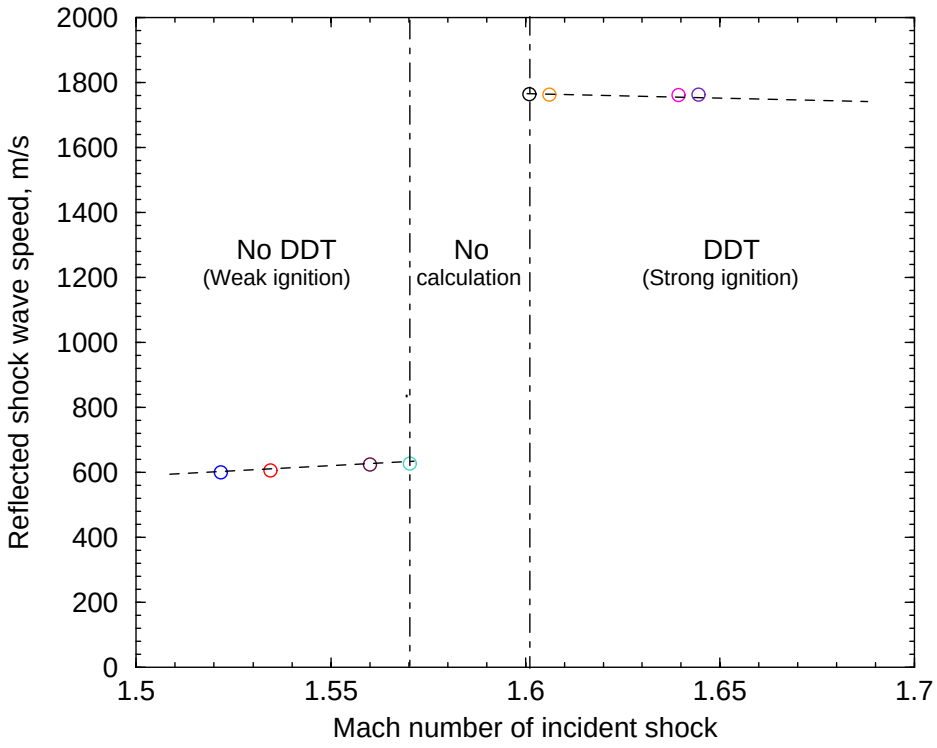

Figure 6.2.3: Calculated diagram of incident shock Mach number versus reflected wave speed

6.3 Comparison between experiment and calculation

Comparing the calculations and experiments, it can be concluded that COM3D with the new reduced chemistry model can predict the occurrence of DDT if the incident shock Mach number is not in the transition zone and not very close to it. Table 2 and Table 3 show that the calculations successfully predicted the occurrence of a strong detonation like ignition in the cases of R0601_15, 16,17, 20, 21 and 23, but failed for R0601_19 and 22, for which the incident shock Mach numbers are in the transition zone. In principle, experiments in this region are not reproducible. In Figure 6.3.1, a pair of symbols with the same color stands for an experimental point (a cross) and a calculated point (a circle) under the same initial condition and configuration. This plot shows that the circles are close to the corresponding cross with the same color, except the indigo ones and orange ones, which are located in the experimentally found transition zone.

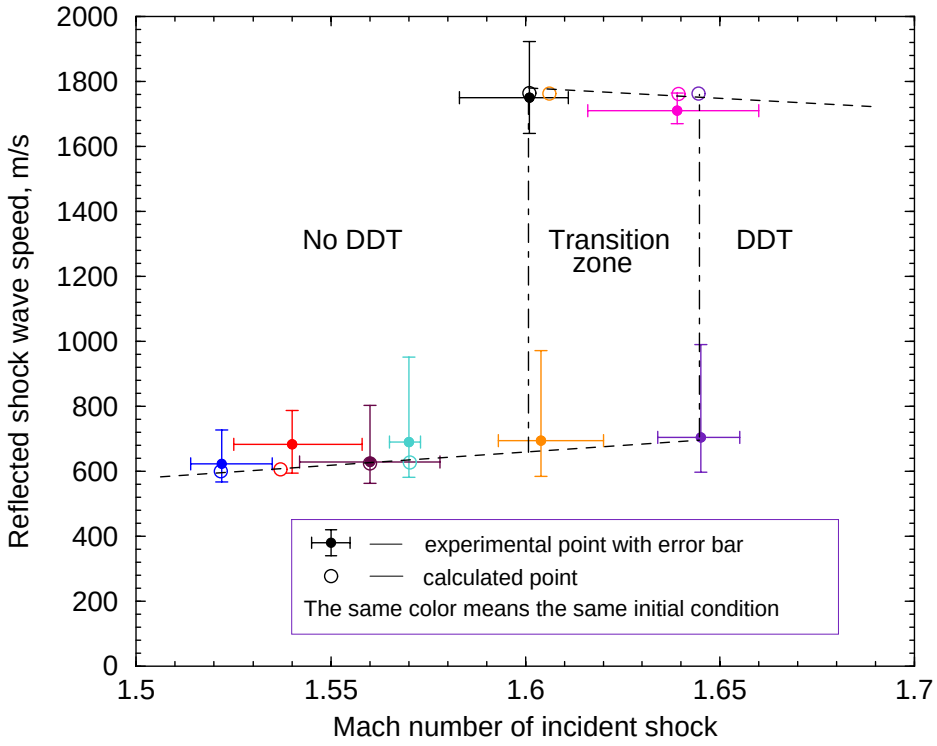

Figure 6.3.1: Comparison between measured and calculated reflected shock wave speeds

6.4 Detailed comparison of deflagrative and detonative ignitions

The simulations using the new COM3D version also allowed a closer look to the differences between deflagrative and detonative ignitions. R0601_15 is taken as an example for DDT, and R0601_21 as an example without DDT.

6.4.1 Pressure distributions

The pressure distributions along the tube at different times are shown in Figure 6.4.1 and Figure 6.4.2 respectively. The two red boundaries stand for the initial profile at 0 ms, and the last profile at 3.6 ms in Figure 6.4.1, or at 4.97 ms in Figure 6.4.2, respectively. Comparing the two figures, the incoming shock wave fronts are very similar to each other in both cases. However the reflected shock waves have quite different amplitudes, the detonation wave amplitude is much higher than the deflagration one. The detonation shocks always have the highest pressure in the front moving away from the reflector. Contrarily, the highest pressures of the deflagration waves exist near the corner of the wedge until the pressure at the corner decays to a certain value. The three dimensional profiles are shown in Figure 6.4.3 and Figure 6.4.4, in which the shock fronts and the contact surface between the reactive mixture and the inert gas can be clearly recognized.

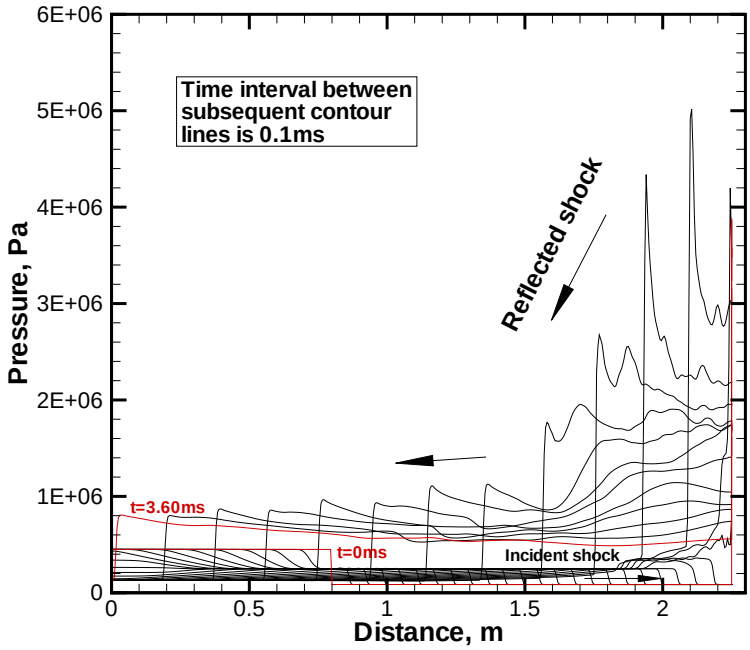

Figure 6.4.1: Calculated pressure profiles along the tube for test R0601_15 (case with DDT)

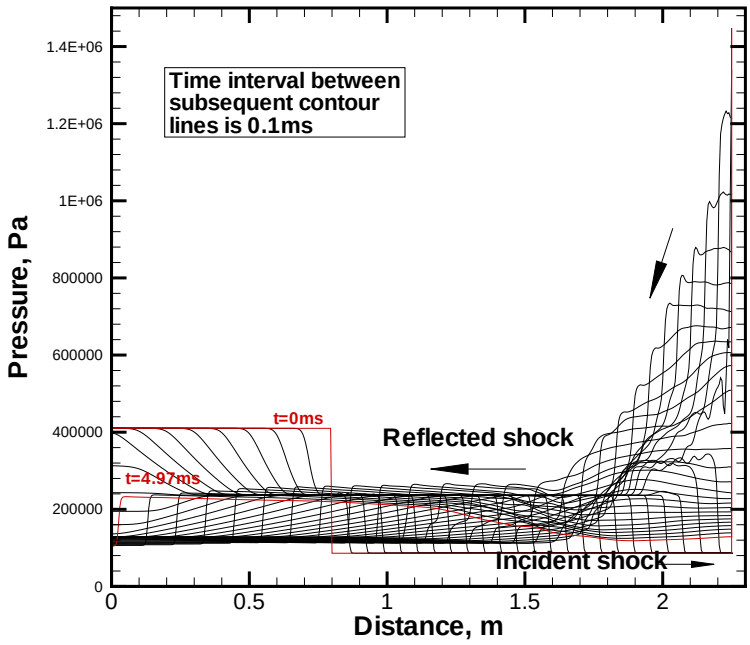

Figure 6.4.2: Calculated pressure profiles along the tube for test R0601_21 (case without DDT)

Figure 6.4.3: 3D-plot for calculated pressure profiles in test R0601_15 (case with DDT)

Figure 6.4.4: 3D-plot for calculated pressure profiles in test R0601_21 (case without DDT)

6.4.2 Temperature distributions

Figure 6.4.5 and 6.4.6 compare the calculated temperature profiles along the tube for both cases. The distinct features of the two ignition models are obvious from the two plots. In case of DDT the temperature profiles show typical detonation values and shape until the detonation front reaches the contact surface, leading to quenching of the chemical reaction and further shock propagating into the gas moving from left to right. For experiment R0601_21, for which no DDT was observed, the COM3D calculation predicts temperatures below 700 K, and consequently only a weak chemical reaction which is too slow to couple to the reflected shock front leaving the reflector.

It is of much interests how the temperature develops locally in the wedge space in both cases. Thus the temperature profiles in the wedge space with a very fine time step are shown in Figure 6.4.7 and Figure 6.4.8. Comparing the two cases, the temperature developments are very similar to each other before the incoming shock front arrives exactly at the end of the wedge. Immediately after this event, the system temperature rises dramatically up to about 2700 K in the case of R0601_15, while the temperature in the case of R0601_21 does not rise above 700 K. In the first case, a coherent local explosion is predicted in the corner of the wedge. In the final region, about 2.5 cm long, of the wedge volume the mixture reacts rapidly and completely within a few 10^{-5} seconds (from 2.39 ms to 2.41 ms). This local explosion of a sizable amount of H_2-air mixture triggers a strong shock front with sufficiently high temperatures for further fast chemical reaction and onset of a stable detonation front. Contrarily, in test R0601_21 (Figure 6.4.8), this local explosion does not occur and the predicted temperatures remain below 700 K. The transition to detonation has been completed in the case of R0601_15, but not in the case of R0601_21. The temperature profiles are also shown in Figure 6.4.9 and Figure 6.4.10 in three-dimensional form.

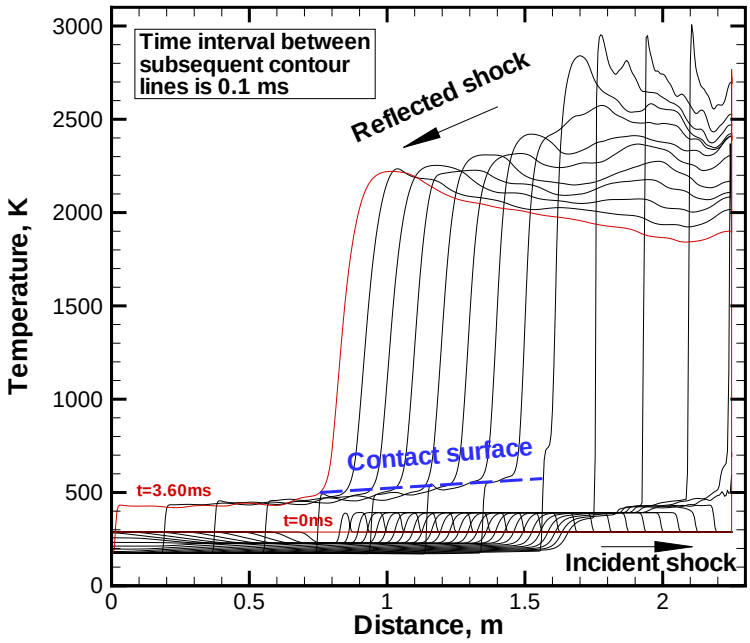

Figure 6.4.5: Calculated temperature profiles along the tube for test R0601_15 (case with DDT)

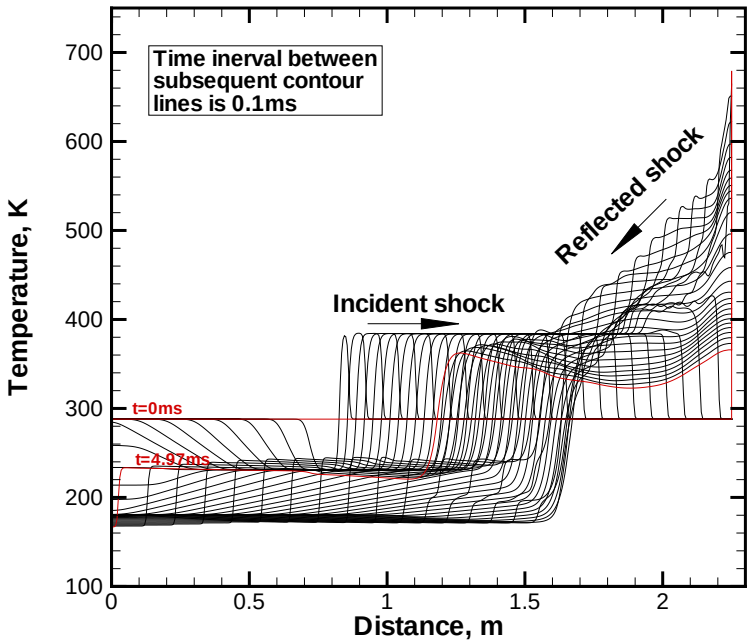

Figure 6.4.6: Calculated temperature profiles along the tube for test R0601_21 (case without DDT)

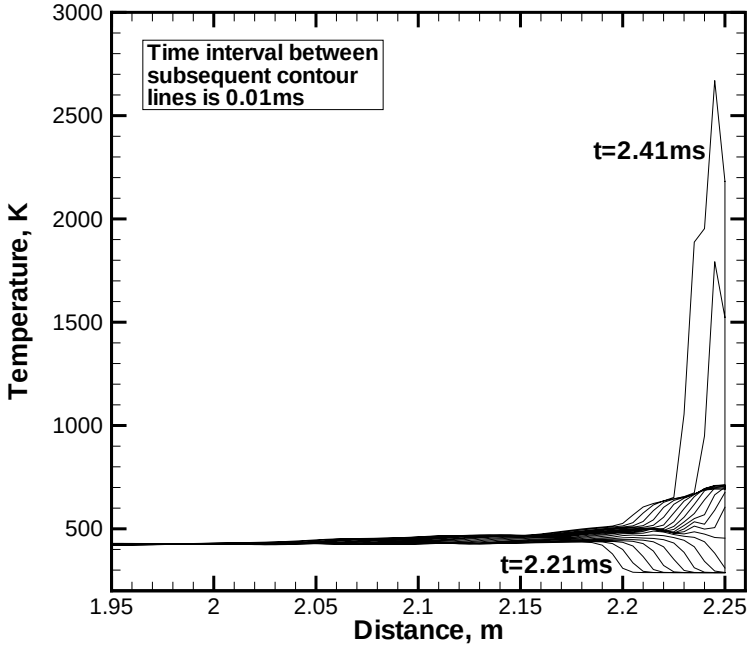

Figure 6.4.7: Calculated temperature profiles in the wedge space for test R0601_15 from 2.21 ms to 2.41 ms, the duration around the time of arrival of incident shock front at the end (2.25 m) of the wedge-shaped reflector. Local explosion occurs between 2.39 ms and 2.41 ms

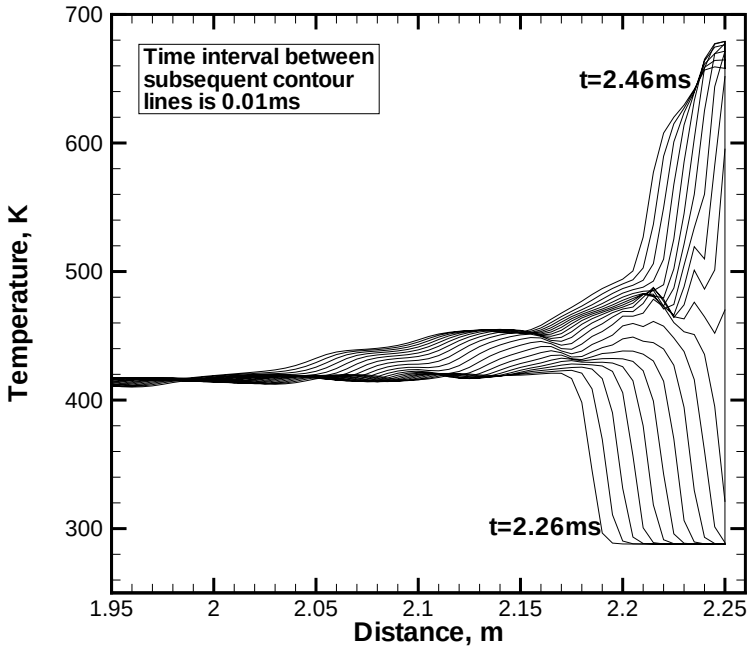

Figure 6.4.8: Corresponding calculated temperature profiles in the wedge space for test R0601_21 from 2.26 ms to 2.46 ms, no DDT

Figure 6.4.9: 3D-plot for calculated temperature profiles in test R0601_15 (case with DDT)

Figure 6.4.10: 3D-plot for calculated temperature profiles in test R0601_21 (case without DDT)

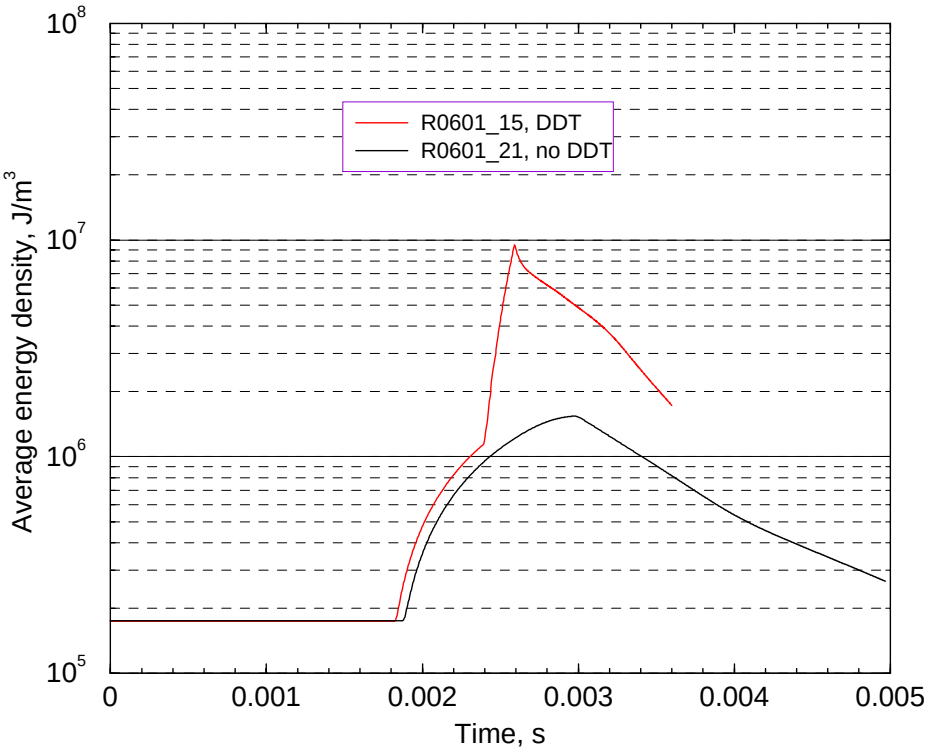

Figure 6.4.11: Calculated average energy density history in the wedge gas volume

6.4.3 Energy density in the wedge gas volume

The history of the average energy density in the wedge gas volume is shown in Figure 6.4.11. For both cases with and without DDT, the profiles are very similar to each other in the induction phase. However the energy density in the case of R0601_15 is about 20-30% higher at given time than that of R0601_21. This difference seems to be a very critical factor determining the ignition regime. The higher energy density results in a strong ignition and a detonation in R0601_15, in which a large amount of additional energy is emitted from the acute chemical reaction. The rapid chemical reaction increases the average energy density in the wedge gas volume by almost a factor of 10 within 0.3 ms, compared to the weak ignition case (R0601_21). The lower energy density in R0601_21 leads only to a mild deflagrative ignition.

6.5 Behavior of the radical H

The radical H is an important species in the hydrogen-oxygen chemistry, therefore it is explicitly described in the reduced chemical model of the updated COM3D code. The two-dimensional distributions of the radical H and the pressure distribution are recorded in Figure 6.4.12 using R0601_15 as an example for DDT again.

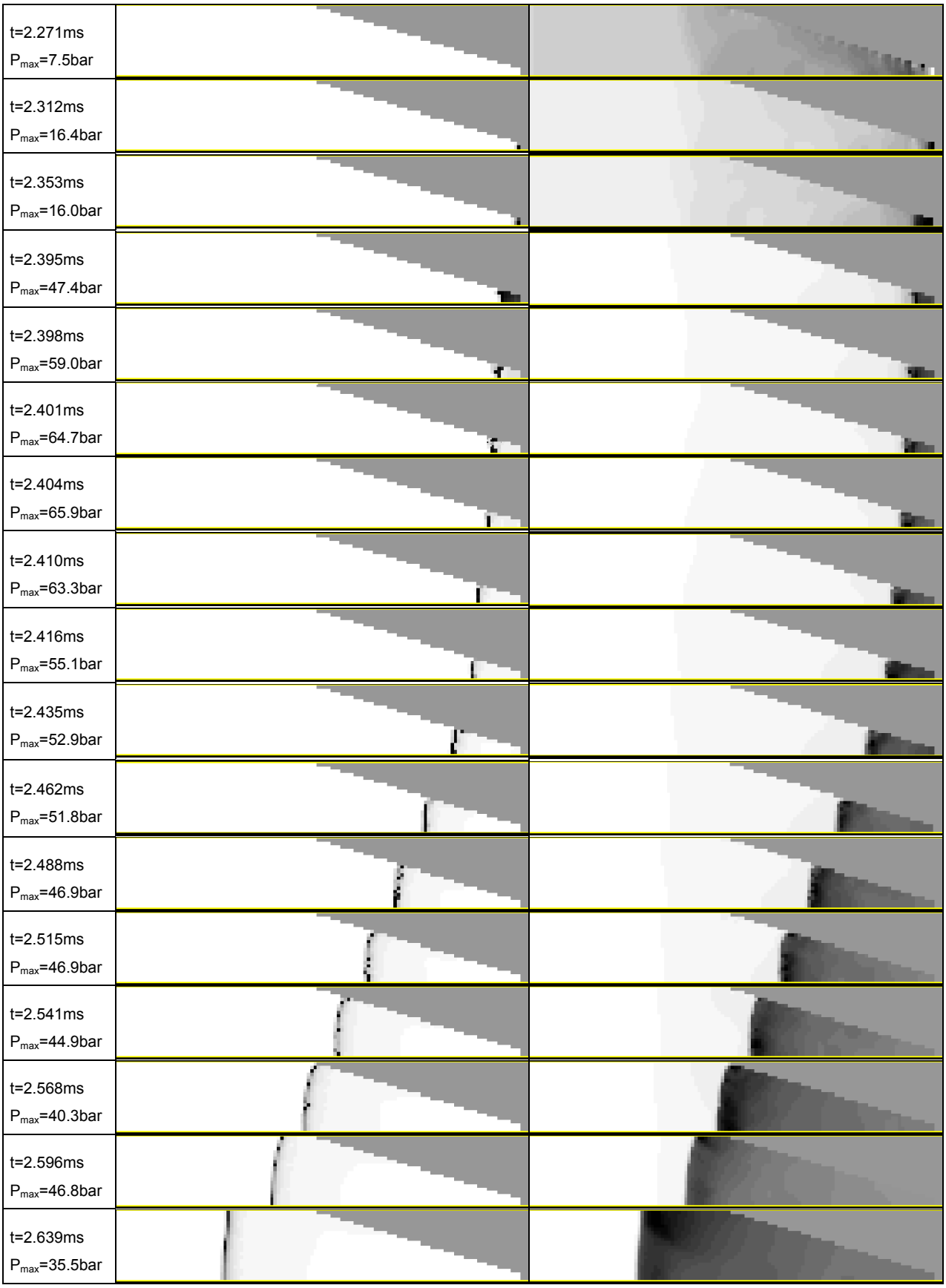

Figure 6.4.12: Numerical simulation of experiment R0601_15, showing the distributions of the radical H (left) and the pressure (right). A local explosion at 2.395 ms triggers a stable detonation front moving to the left, out of the wedge

In the figure, the first column records the time and the system peak pressure when the pictures are recorded. The second column records the distribution of radical H concentration, and the third column records the pressure distribution. According to the figure, a visual quantity of radical H begins to appear in the corner when the incident shock arrives at the corner (2.312 ms). The chemical reaction spreads rapidly from this initial kernel and within about 80 μs a coherent local explosion occurs in the wedge corner (2.395 ms). The peak pressure jumps from about 16 bar to 47 bar. From there on the chemical reaction proceeds mainly in the leading shock moving out of the wedge. This coupled reaction front, the propagation speed and the pressure distribution behind the shock front are typical for a detonation wave.

7. Conclusions

In this paper a new approach for reduction of the detailed hydrogen-oxygen chemistry is presented. The main objective was to develop a fast-running, but still sufficiently precise scheme for use in three dimensional CFD programs.

A two-step model was chosen because this allows the simplest possible representation of the chain-branching reaction which builds up a radical pool (first step) and of the chain-terminating reaction (second step). The reaction rate constants for these two model reactions were derived from a detailed seven-step model and fitted in the form of fast evaluating polynomials using 8 and 17 terms, respectively. The applicability range of the derived polynomials covers any lean to stoichiometric hydrogen-air mixtures with initial temperatures from 300 to 3000 K, and initial pressures from 0.5 to 50 bar. Comparison between the new reduced model and the detailed model showed good agreements for the induction time and the reaction time. The differences are of the magnitude as the differences found between different detailed schemes found in current literatures.

The new reduced chemistry model was implemented into the COM3D code as a modular subroutine. Various test calculations demonstrated numerical stability, convergence and fast running performance of the new chemistry model (+1.3% CPU-time compared to a single-step Arrhenius model).

The physical correctness and predictability of the model was evaluated by comparison to a quite complicated problem of reactive flow, namely focusing of a shock wave in a converging target geometry and subsequent weak or strong ignition of the used hydrogen-air mixture (start of a slow deflagration or ignition of a detonation). A special set of experiments were performed in a rectangular shock tube facility. Depending on the Mach number of the incident shock, a region with weak ignition, with strong ignition and a transition region where both processes are possible, could be identified. The simulation of these tests demonstrated that the code with the new reduced chemistry model could reproduce all essential features of the experiments in a very satisfactory way (e.g. Figure 6.3.1). The code calculation allowed also detailed insights into the microscopic processes. In case of the strong detonative ignition a local explosion in the reflector triggers the on-set of the stable detonation wave.

It may be concluded that the new COM3D version with adequate space and time resolution can correctly predict the dynamics of a large range of hydrogen-oxygen combustion regimes, from slow deflagrations to detonations.

Acknowledgment

The authors do appreciate Dr. W. Breitung and Dr. B. Burgeth for many fruitful discussions about the work. Additionally the authors do feel grateful to A. Veser, G. Stern and J. Grune for their experimental contributions. Many thanks to V. Krautschick for his contribution to translate the abstract of this report into German.

References

[1] Maas, U., Pope, S. B., Twenty-Fourth Symposium (International) on Combustion / The Combustion Institute, 1992/pp. 103-112.

[2] Reduced Kinetic Mechanisms and Asymptotic Approximations for Methane-Air Flames (M. D. Smooke, Ed.), Lecture Notes in Physics 384, Springer (1991).

[3] Eggels, R. L. G. M., Goey, L. P. H., Combustion and Flame, 100:559-570 (1995).

[4] Balakrishnan, G., Smooke, M. D., Williams, F. A., Combustion and Flame, 102:329-340 (1995).

[5] Seshadri, K., Peters, N., Williams, F. A., Combustion and Flame, 96:407-427 (1994).

[6] Ju, Y., Niioka, T., Combustion and Flame, 99:240-246 (1994).

[7] Montgomery, C. J., Kosaly, G., Riley, J. J., Combustion and Flame, 109:113-144 (1997).

[8] Sohn, C. H., Chung, S. H., Lee, S. R. et al, Combustion and Flame, 115:299-312 (1998).

[9] He, L., Paul, C., Combustion and Flame, 93:391-407 (1993).

[10] García-Ybarra, P. L., Treviño, C., Combustion and Flame, 96:293-303 (1994).

[11] Sánchez, A. L., Liñán, A., Williams, F. A., Combustion Science and Technology, 1997, Vol. 123, pp. 317-345.

[12] Kim, Y. M., Kim, H, J., Combustion Science and Technology, 1998, Vol. 137, pp. 51-80.

[13] Maas, U., Pope, S. B., Combustion and Flame, 88:239-264 (1992).

[14] Breitung, W., Veser, A., Stern, G., private communication (2001).

Appendix I

Arrhenius parameters of the detailed 7-step scheme [3]

$$k = AT^{\beta} \exp(-E / RT)$$

Reaction	Forward			Backward		
	A (in units of mol/cm^3, s^{-1})	β	E (J/mol)	A (in units of mol/cm^3, s^{-1})	β	E (J/mol)
$H+O_2 \Leftrightarrow OH+O$	0.2000E+15	0.00	70300	0.1460E+14	0.00	2080
$O+H_2 \Leftrightarrow OH+H$	0.5060E+05	2.67	26300	0.2240E+05	2.67	18400
$H_2+OH \Leftrightarrow H_2O+H$	0.1000E+09	1.60	13800	0.4450E+09	1.60	77130
$OH+OH \Leftrightarrow O+H_2O$	0.1500E+10	1.14	420	0.1510E+11	1.14	71640
$H+H+M \Leftrightarrow H_2+M$	0.1800E+19	-1.00	0	0.6990E+19	-1.00	436080
$OH+H+M \Leftrightarrow H_2O+M$	0.2200E+23	-2.00	0	0.3800E+24	-2.00	499410
$O+O+M \Leftrightarrow O_2+M$	0.2900E+18	-1.00	0	0.6810E+19	-1.00	496410

Chaperon coefficients: H_2O/6.5/ H_2/1.0/ N_2/0.5/ O_2/0.35/

Appendix II

Coefficients of the polynomial fittings

i	c_{fi}	c_{bi}	d_{fi}	d_{bi}
1	-2.478446051575132e+00	-1.550943081568231e+00	1.366520282229579e+01	3.628623007697461e+00
2	-8.520562063932220e-07	1.404276122758379e-04	3.588311008324488e-02	2.273306278479073e-02
3	-2.999410469345436e+00	5.105296691026530e-03	-8.572213866474634e-04	-6.561954987738053e-04
4	3.987325135947901e+01	7.498474881040089e+00	4.416979842300994e-06	3.474095191345424e-06
5	4.111966238789625e-02	3.315924650253477e-02	-2.581631067783013e-02	-6.588757749814234e-03
6	-1.148785078687674e-05	-1.057940084838372e-05	1.111679800176949e-05	1.658523394696077e-06
7	1.579827766792452e-09	1.536490108678185e-09	-1.483794436728837e-09	-1.092150135172017e-10
8	-8.404434944349489e-14	-8.416101705419116e-14	-8.769479747749635e+00	-1.996998807307908e+00
9			7.654637552623472e-03	-8.117419136350834e-06
10			-2.813276043466464e-06	1.476530720969605e-07
11			3.502525601707695e-10	-3.481568935446353e-11
12			-5.182605108493024e-05	-7.331529164799113e-06
13			-4.665586162744686e+02	-4.302597752220542e+02
14			8.455342514733113e+01	6.948745878611116e+01
15			1.551841209732263e+04	6.691869175776566e+04
16			-2.824670074880856e+00	-1.606421033059446e+00
17			8.899146681010474e+06	-9.734021744497530e+06